abd-2

AD

USAAVLABS TECHNICAL REPORT 71-7

DETERMINATION OF PHYSICAL AND STRUCTURAL PROPERTIES OF MIXED-MODULUS COMPOSITE MATERIALS

By

Robert L. Pinckney
Richard B. Freeman

June 1971

EUSTIS DIRECTORATE
U. S. ARMY AIR MOBILITY RESEARCH AND DEVELOPMENT LABORATORY
FORT EUSTIS, VIRGINIA

CONTRACT DAAJ02-69-C-0059
VERTOL DIVISION
THE BOEING COMPANY
PHILADELPHIA, PENNSYLVANIA

75

Unclassified

Security Classification

DOCUMENT CONTROL DATA - R & D

(Security classification of title, body of abstract and indexing annotation must be entered when the overall report is classified)

1. ORIGINATING ACTIVITY (Corporate author)	2a. REPORT SECURITY CLASSIFICATION
Vertol Division The Boeing Company Philadelphia, Pennsylvania	Unclassified 2b. GROUP

3. REPORT TITLE

DETERMINATION OF PHYSICAL AND STRUCTURAL PROPERTIES OF MIXED-MODULUS COMPOSITE MATERIALS

4. DESCRIPTIVE NOTES (Type of report and inclusive dates)

Final Report

5. AUTHOR(S) (First name, middle initial, last name)

Robert L. Pinckney
Richard B. Freeman

6. REPORT DATE	7a. TOTAL NO. OF PAGES	7b. NO. OF REFS
June 1971	75	

8a. CONTRACT OR GRANT NO.	9a. ORIGINATOR'S REPORT NUMBER(S)
DAAJ02-69-C-0059 b. PROJECT NO. c. Task 1F162204A17003 d.	USAAVLABS Technical Report 71-7 9b. OTHER REPORT NO(S) (Any other numbers that may be assigned this report) D210-10196-1

10. DISTRIBUTION STATEMENT

Approved for public release; distribution unlimited.

11. SUPPLEMENTARY NOTES	12. SPONSORING MILITARY ACTIVITY
	Eustis Directorate U.S. Army Air Mobility R&D Laboratory Fort Eustis, Virginia

13. ABSTRACT

The objective of this program was to determine the physical and structural properties of mixed-modulus composite materials using combinations of graphite and S-glass fibers under static and fatigue loading conditions.

This report covers the work completed under Phase I and Phase II of the program and summarizes the data obtained for solid laminates, tubular specimens and sandwich beams in which the S-glass material was oriented parallel to the longitudinal axis of the specimens and the graphite fibers were oriented at $\pm 45^{\circ}$ to the same axis.

The test results are tabulated in appropriate engineering format. S-N curves are included to illustrate the fatigue performance of the materials. Stress-strain and S-N curves are compated to appropriate data on pure S-glass and pure graphite material where such data contributes to an understanding of the mixed materials performance.

The data indicates that the mixed-modulus system of S-glass and graphite is compatible with the structural and failure mode requirements of helicopter rotor blades.

DD FORM 1 NOV 68 1473 REPLACES DD FORM 1473, 1 JAN 64, WHICH IS OBSOLETE FOR ARMY USE.

Unclassified

Security Classification

DISCLAIMERS

The findings in this report are not to be construed as an official Department of the Army position unless so designated by other authorized documents.

When Government drawings, specifications, or other data are used for any purpose other than in connection with a definitely related Government procurement operation, the United States Government thereby incurs no responsibility nor any obligation whatsoever; and the fact that the Government may have formulated, furnished, or in any way supplied the said drawings, specifications, or other data is not to be regarded by implication or otherwise as in any manner licensing the holder or any other person or corporation, or conveying any rights or permission, to manufacture, use, or sell any patented invention that may in any way be related thereto.

Trade names cited in this report do not constitute an offical endorsement or approval of the use of such commercial hardware or software.

DISPOSITION INSTRUCTIONS

Destroy this report when no longer needed. Do not return it to the originator.

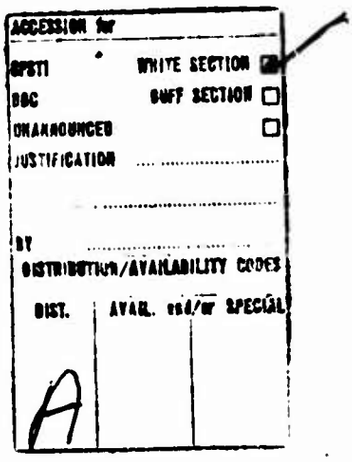

14. KEY WORDS	LINK A		LINK B		LINK C	
	ROLE	WT	ROLE	WT	ROLE	WT
Mixed-modulus composites						
Graphite angle-ply composite						
S-glass unidirectional composite						
Laminate fabrication						
Sandwich fabrication						
Tube fabrication						
Fatigue testing						
Creep testing						
Failure Analysis						

DEPARTMENT OF THE ARMY
U. S. ARMY AIR MOBILITY RESEARCH & DEVELOPMENT LABORATORY
EUSTIS DIRECTORATE
FORT EUSTIS, VIRGINIA 23604

This program was carried out under Contract DAAJ02-69-C-0059 with the Vertol Division of The Boeing Company.

The objective of the program was to determine the physical and structural properties of mixed-modulus composite materials using combinations of graphite and S-glass fibers under static and fatigue loadings.

This directorate has reviewed the report and considers the research reported to be a step forward in improving aircraft structures. The report is published for the exchange of information and the stimulation of future research.

The technical monitor for this contract was Mr. I. E. Figge, Structures Division.

Task 1F162204A17003
Contract DAAJ02-69-C-0059
USAAVLABS Technical Report 71-7
June 1971

DETERMINATION OF PHYSICAL AND STRUCTURAL PROPERTIES OF MIXED-MODULUS COMPOSITE MATERIALS

Final Report

D210-10196-1

By

Robert L. Pinckney
Richard B. Freeman

Prepared by

Vertol Division
The Boeing Company
Philadelphia, Pennsylvania

for

EUSTIS DIRECTORATE
U. S. ARMY AIR MOBILITY RESEARCH AND DEVELOPMENT LABORATORY
FORT EUSTIS, VIRGINIA

SUMMARY

The objective of this program was to determine the physical and structural properties of mixed-modulus composite materials using combinations of graphite and S-glass fibers under static and fatigue loading conditions.

This report covers the work completed under Phase I and Phase II of the program and summarizes the data obtained for solid laminates, tubular specimens and sandwich beams in which the S-glass material was oriented parallel to the longitudinal axis of the specimens and the graphite fibers were oriented at $\pm 45°$ to the same axis.

The test results are tabulated in appropriate engineering format. S-N curves are included to illustrate the fatigue performance of the materials. Stress-strain and S-N curves are compared to appropriate data on pure S-glass and pure graphite material where such data contributes to an understanding of the mixed materials performance.

The data indicates that the mixed-modulus system of S-glass and graphite is compatible with the structural and failure mode requirements of helicopter rotor blades.

TABLE OF CONTENTS

LIST OF ILLUSTRATIONS

LIST OF TABLES

BLANK PAGE

INTRODUCTION

The use of fiber reinforced composite materials has increased rapidly in the past few years. Significant progress has been made since 1960 in the development of composite materials and their utilization in advanced aerospace and deep submergence structures.

The development of S-glass, and its successful incorporation in primary structure of Minuteman and Polaris vehicles, gave structures and design engineers a new engineering material having favorable static and fatigue strength-to-weight ratios.

Many materials in the past have been used for advanced structures. Each of these materials in time has shown its limitation. For example: the weight of steel structures essentially limits their application; the strength of aluminum structures turns out to be their limiting factor; magnesium has environmental or corrosion problems; and conventional aluminosilicate and borosilicate glass materials turn out to be essentially modulus limited.

Although extensive work has been conducted on improving the modulus of glass fiber materials, the tensile and flexural stiffness of glass fibers is not expected to rise much above 20 million pounds per square inch in the foreseeable future.

More recent developments in the area of fiber reinforcements have produced two materials having significantly improved modulus properties. Tungsten-core boron fibers now consistently show a fiber tensile modulus above 58 million psi, with a favorable strength-to-weight ratio, and graphite and carbon fibers have moduli of 25 to 80 million psi. The combination of these three materials -- glass, graphite, and boron -- appears to hold the most significant promise for application in this decade.

With this consideration in mind, the program pursued the following objectives:

- Evaluate new mixed reinforcement and proven resin matrix materials as composite constituents.

- Determine the compatibility of, and the elastic properties of, multi-ply materials having varying fiber properties and orientations.

- Compare the elastic and strength properties of combined mixed-fiber material to its constituent composites.

- Define property interactions where necessary, and validate established methods and procedures of specimen fabrication, instrumentation, and property measurement, utilizing mixed-modulus composite materials.

DISCUSSION OF TEST RESULTS

PROGRAM TEST PLAN

The program was broken down into two phases, as shown in Tables I and II. Phase I was directed at obtaining basic strength, fatigue response, and failure modes of the mixed-modulus materials system. Since Phase I provided acceptable results, Phase II was pursued, (Table II), with its objective being to look more closely at the constitutents of the mixed-modulus system to obtain a better understanding of its reponse. Upon conclusion of Phases I and II, the test matrix, as shown in Figure 1, was complete, and appropriate material performance comparisons could be made.

The prepreg materials, Owens Corning's S-glass impregnated with 1002 epoxy resin supplied by the 3M Company and Courtaulds HM-S (high-modulus, surface-treated) graphite fiber impregnated with American Cyanamid's BP907 resin, were utilized during this program. The mixed-modulus system consisted of 0°, unidirectional S-glass-1002 resin along with $\pm$45° graphite-BP907 resin. The particular precentages of 0° and $\pm$45° material used for the laminates, tubes and sandwich beams can be determined from the appropriate layups, which are presented in Tables I and II, along with the fact that the per-ply thicknesses are 0.0093 and 0.0098 inch for S-glass-1002 resin laminates and tubes, respectively,and 0.0074 and 0.0086 inch for the corresponding graphite-BP907 resin values.

LAMINATE FABRICATION

All laminate specimens, utilizing both of the above prepregs, were fabricated in a single-stage cure process utilizing the parameters shown in Figure 2. The specimens were cut with a diamond wheel and machine ground to insure defect-free edges. All laminates used in this program were 1/2 inch wide and constructed per Figure 3, while the interlaminar shear specimens were constructed per Figure 4.

LAMINATE TESTING

Static Tension and Shear Tests

The static laminate tensile tests were performed on either a Baldwin or an Instron test machine at a crosshead speed of 0.05 inch per minute. Elongation and tensile modulus were determined from a mounted extensometer. Figure 5 presents a typical stress*-strain curve for the mixed-modulus specimen as well as

*All stress values calculated for the mixed-modulus composite were based on a gross area which included the total glass and graphite-epoxy cross-sectional areas.

TABLE I. TESTING MATRIX FOR MIXED-MODULUS PROGRAM - PHASE I

TYPE OF SPECIMEN	MATERIAL	TOTAL NO. OF PLIES	FIBER ORIENTATION AND LAY-UP	NO. OF TEST SPECIMENS	TYPE OF TEST
Laminate	Graphite	17	17 plies uni par. to long. axis	6	
	S-Glass	17	Same as above	6	Static Inter-
	Graphite		5 plies uni par. to long. axis		laminar
	S-Glass	13	3 plies uni par. to long. axis	6	Shear
	Graphite		5 plies uni par. to long. axis		
Laminate	Graphite		3 plies $\pm$45° to long. axis		Static
	S-Glass	16	10 plies uni par. to long. axis	6	Canti-
	Graphite		3 plies $\pm$45° to long. axis		lever
			(+,-,+,0_{10},-,+,-)		Deflec.
Laminate	Graphite		3 plies $\pm$45° to long. axis		Static
	S-Glass	16	10 plies uni par. to long. axis	5	Tensile
	Graphite		3 plies $\pm$45° to long. axis		Ultimate
			(+,-,+,0_{10},-,+,-)		
Sandwich	Graphite	4 per	2 plies $\pm$45° to long. axis		Static
Beam	S-Glass	skin	2 plies uni par. to long. axis	5	Bending
			(+,-,0,0,core,0,0,-,+)		Ultimate
Sandwich	Graphite	4 per	2 plies $\pm$45° to long. axis		Bending
Beam	S-Glass	skin	2 plies uni par. to long. axis	19	Fatigue
			(+,-,0,0,core,0,0,-,+)		
Tube	Graphite		2 plies $\pm$45° to long. axis		Static
	S-Glass	7	3 plies uni par. to long. axis	5	Torsional
	Graphite		2 plies $\pm$45° to long. axis		Ultimate
			(+,-,0,0,0,-,+)		
Tube	Graphite		2 plies $\pm$45° to long. axis		
	S-Glass	7	3 plies uni par. to long. axis	15	Torsional
	Graphite		2 plies $\pm$45° to long. axis		Fatigue
			(+,-,0,0,0,-,+)		
Tube	Graphite		2 plies $\pm$45° to long. axis		Torsional
	S-Glass	7	3 plies uni par. to long. axis	5	Fatigue
	Graphite		2 plies $\pm$45° to long. axis		+ Steady
			(+,-,0,0,0,-,+)		Tension

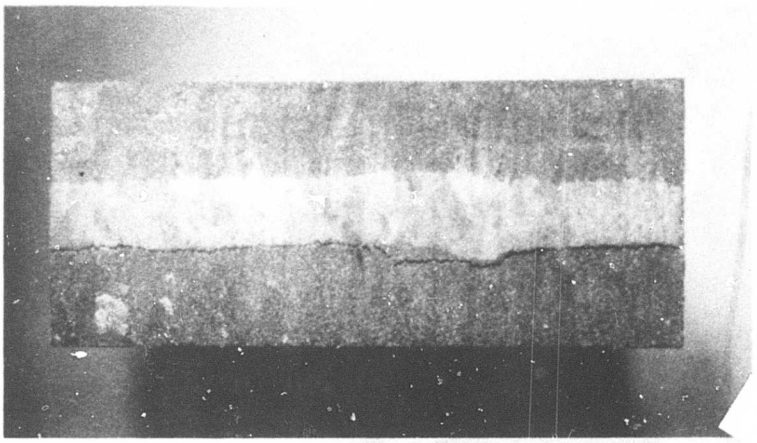

MIXED-MODULUS

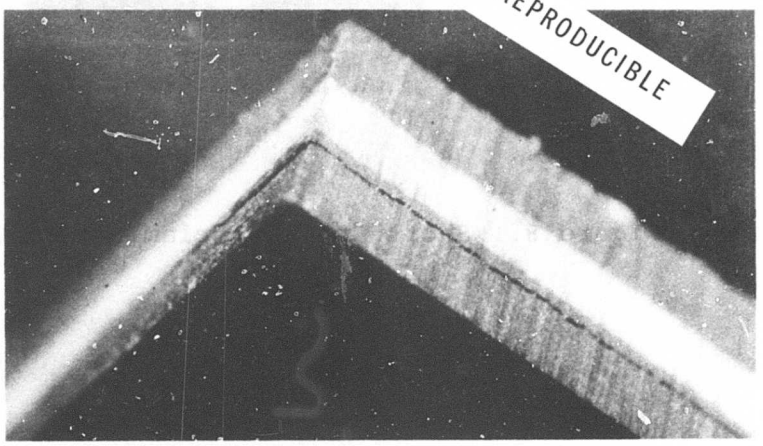

MIXED-MODULUS

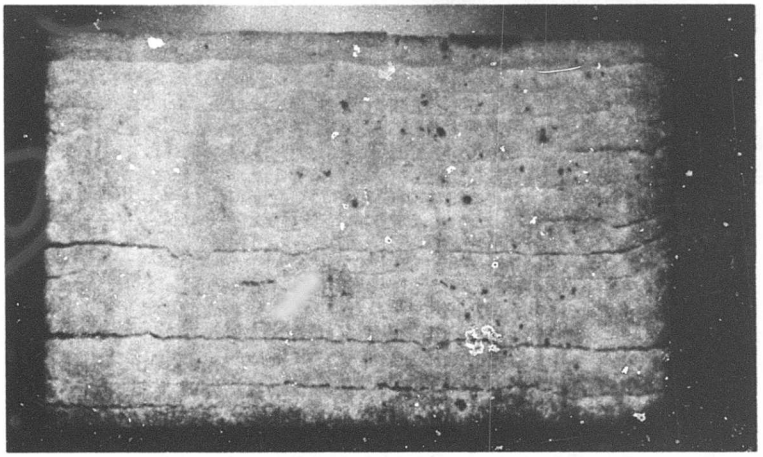

S-GLASS

Figure 7. Typical Failed Short-Beam Interlaminar Shear Specimens.

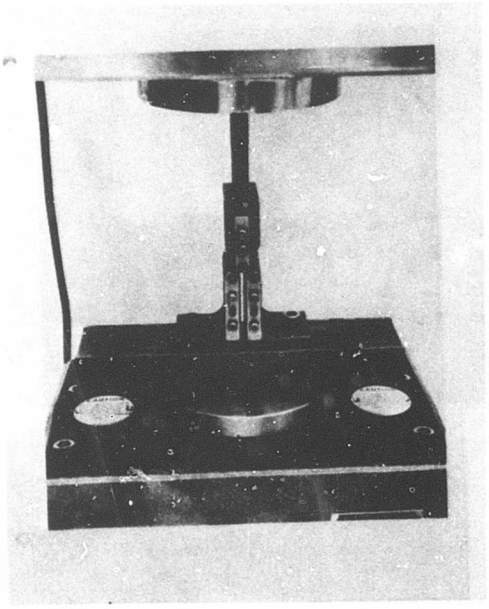

Figure 8. Short-Beam Interlaminar Shear Test Setup.

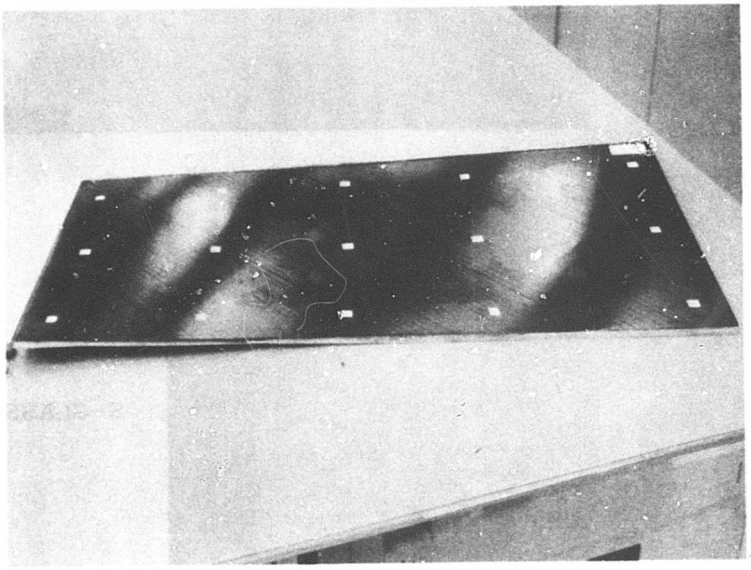

Figure 9. Typical Thermal Distortion of an Unsymmetric Mixed-Modulus Panel.

the case and hence no further tests were made.

Laminate Static Deflection Tests

Static deflection tests were conducted on mixed-modulus specimens 0.50 inch wide by 9.00 inches long which were of the same construction as the thermal distortion panel. The specimens were tested in a 5-kip-capacity Baldwin test machine utilizing a jig which held the specimen as a fixed cantilever beam while a single-point loading was applied (Figure 10). The specimens were deflected at a rate of 0.05 inch/minute to a designated stress level and then unloaded at each of three temperatures (-65°F, +70°F, and +160°F). After unloading, the specimen was checked for damage (i.e., delaminations or permanent set). If no damage was incurred, the designated stress was increased and the loading processes were repeated at each of the three temperatures. The test results for the static cantilever deflection tests are presented in Figure 11.

Laminate Creep Tests

As indicated in Table II, at least three specimens from each of three groups of layup configuration (i.e., all 0°, unidirectional S-glass, all ±45° graphite, and mixed-modulus) were creep tested at +75°F and +160°F. Three load levels for the creep data were initially considered: (1) 90% F_{TU}; (2) 80% F_{TU}; and (3) a representative stress level for a hardware component, which was a rotor blade where the mixed-modulus material is designed to approximately 12.6% of its F_{TU}. In this case, the uni S-glass is loaded to 9.3% of its F_{TU} while the ±45° graphite sees 26.4% of its corresponding F_{TU}.

The creep setup for the ±45° graphite laminates consisted of a dead load frame where the weight was raised and lowered with a hydraulic ram (Figure 12). Figure 13 presents the creep test results for the 80 and 90% F_{TU} loads at +70°F. The +160°F creep test loaded to 80% of the room temperature (R.T.) F_{TU} failed prior to application of the entire load. It had been assumed that the +160°F temperature should reduce the R.T. F_{TU} by only 15% (based on previously conducted tests using boron fiber). The second +160°F graphite specimen was then tested at 60% R.T. F_{TU}, resulting in a creep rupture time of only a few minutes (Figure 13). One of the ±45° graphite laminates which was to be fatigue tested was instead statically failed at +160°F, with the resulting F_{TU} indicating that approximately 40% reduction in R.T. F_{TU} was experienced.

The following sequence was used for both the R.T. and +160°F graphite creep specimens loaded to 26.4% of the R.T. F_{TU}: the load was applied for a day and then unloaded for at least a day; the load was then applied two days and unloaded for at

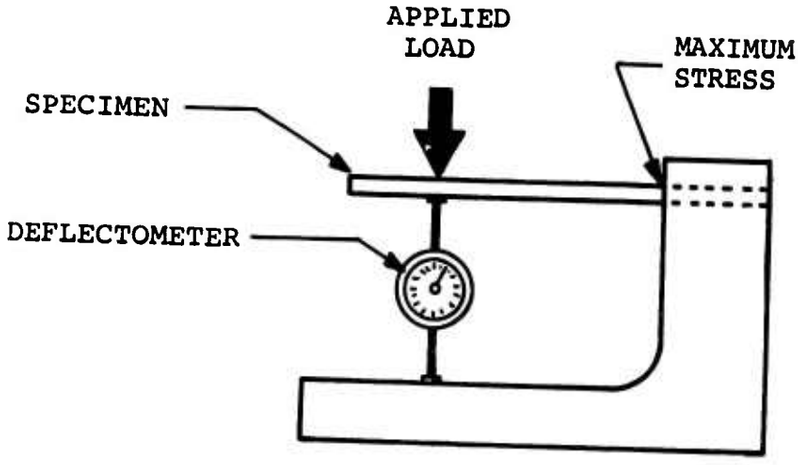

Figure 10. Static Cantilever Deflection Test Setup.

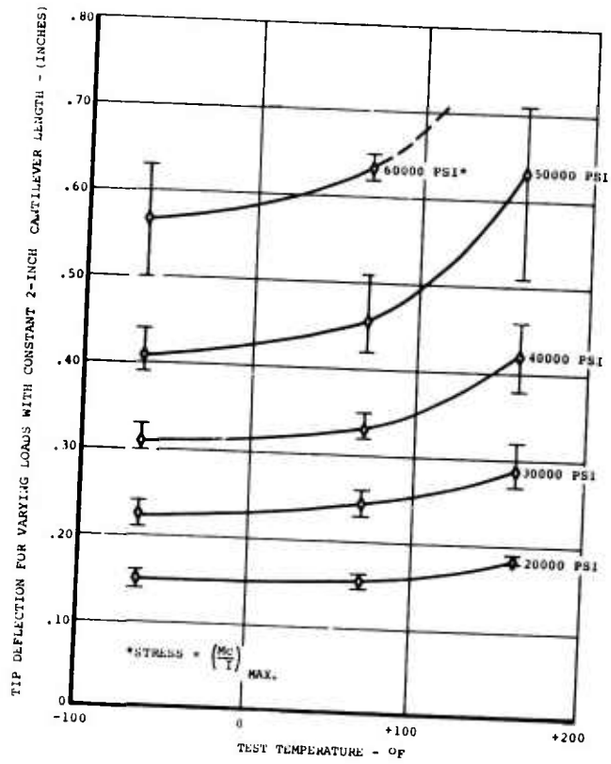

Figure 11. Constant-Load Cantilever Deflection Versus Temperature for Mixed-Modulus Laminate.

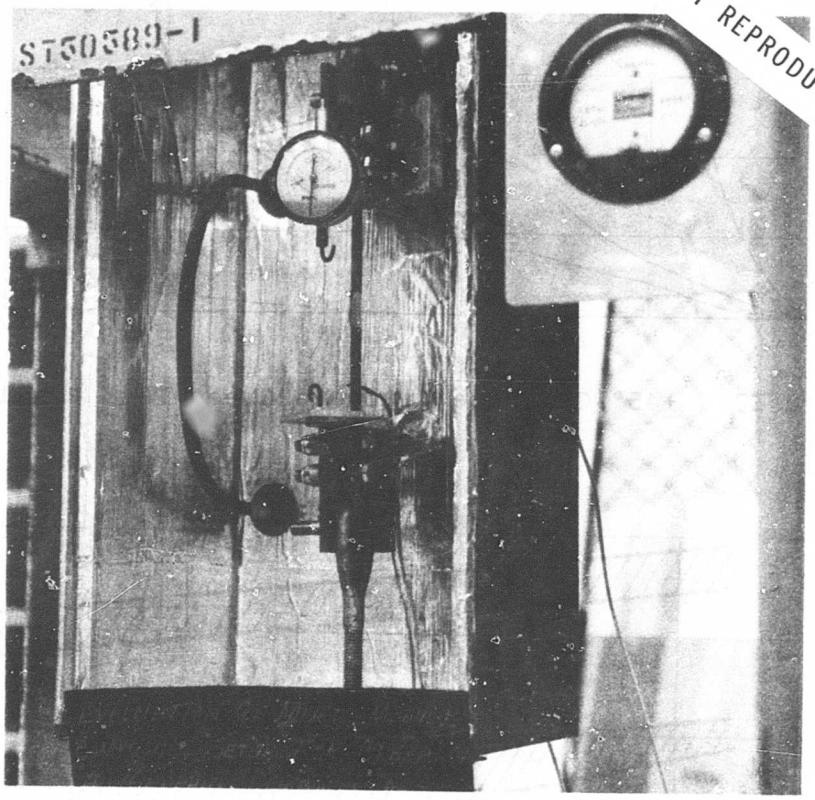

Figure 12. ±45° Graphite Laminate Creep Test Setup.

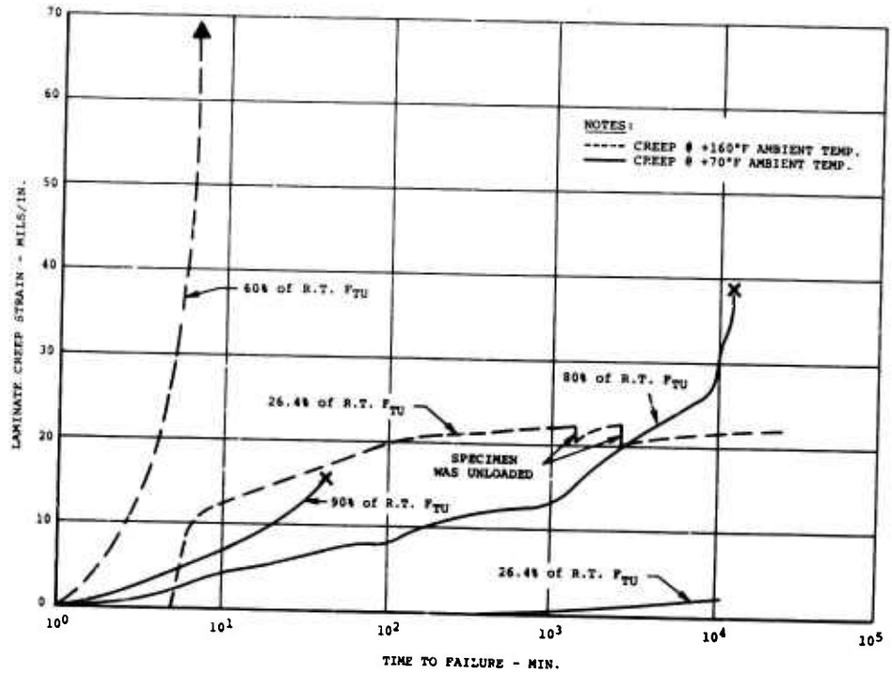

Figure 13. ±45° Graphite Laminate Creep Test Results.

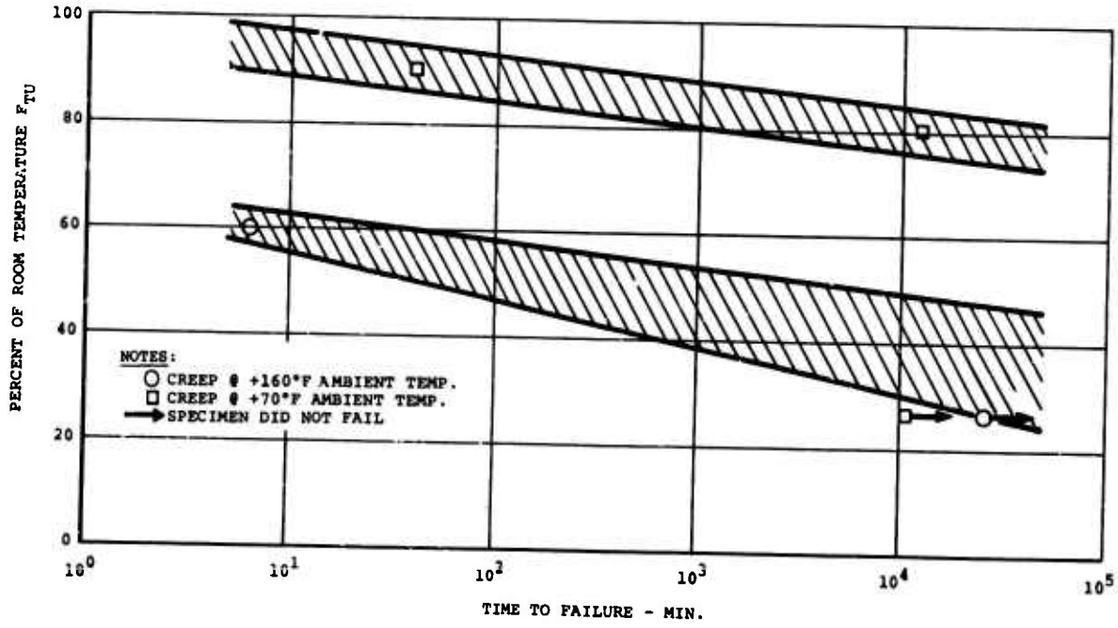

Figure 14. ±45° Graphite Laminate Creep Rupture Test Results.

least a day; and, finally, the load was applied for at least one week. These test results are presented in Figure 13. Figure 14 presents creep rupture curves for the ±45° graphite laminates.

The creep setup for the 0° S-glass laminates consisted of a standard type creep tester where the loads are introduced through a 10:1 multiplying arm and an electric motor is used to load and unload the specimen (Figure 15). A panel of S-glass-1002 resin was fabricated, and 0.50-inch-wide specimens were cut out. Three specimens were statically tested to obtain an average of 229,000 psi. At R.T., the 90% F_{TU} specimen failed prior to application of the entire load. Therefore, test data were taken at 80% and 70% of R.T. F_{TU}. In addition, a 50% F_{TU} was investigated since it was felt that a load of 9.3% F_{TU} (corresponding to a maximum rotor blade load) was too low to observe any creep. Creeps at 80%, 70%, and 50% of R.T. F_{TU} were also conducted at +160°F. The "measured creep" for the 0° S-glass composites occurred in discrete steplike movements which corresponded with visible surface fiber breaking. Because of the mechanism observed and the difficulty in measuring total elongation of the specimen near failure, only the creep-rupture data is presented in Figure 16.

The creep setup for the mixed-modulus laminates was the same as for the 0° S-glass specimens. A problem developed in attempting to load the mixed-modulus specimens to the higher load levels because the graphite angle-ply would fail under the doublers resulting in debonding at the graphite-doubler interface. Note that this problem did not occur in the static tests previously discussed because hydraulic grips were used to provide a constant grip pressure throughout the test -- something the bolted grips of the creep tester could not do -- which helped to prevent the specimen from slipping out from between the doublers. Because of this problem, only the creep at 12.6% of R.T. F_{TU} at +70°F and +160°F was investigated. The resulting creep strain was of an insignificant level.

Dynamic Tension-Tension Testing

In presenting fatigue data, three curves are typically shown. The line labeled "Mean of Test Data" on the S-N curves is the line which best fits the fatigue test data utilizing a least-squares regression line with runout test values omitted. The equation of the least-squares line has the form

$$\log(\text{alternating stress}) = A + B * \text{Log}(\text{number of cycles})$$

where A and B are constants determined by the method of least squares. Using this equation, each data point is transposed parallel with the line to 10^7 cycles, where a standard

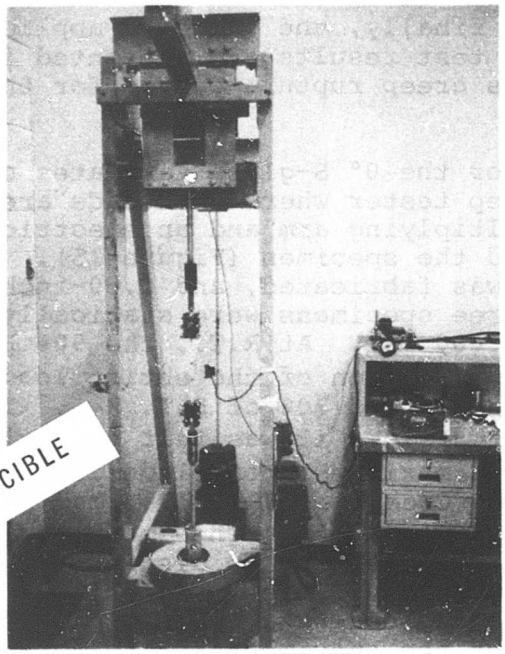

Figure 15. Unidirectional, 0°, S-Glass Laminate Creep Test Setup.

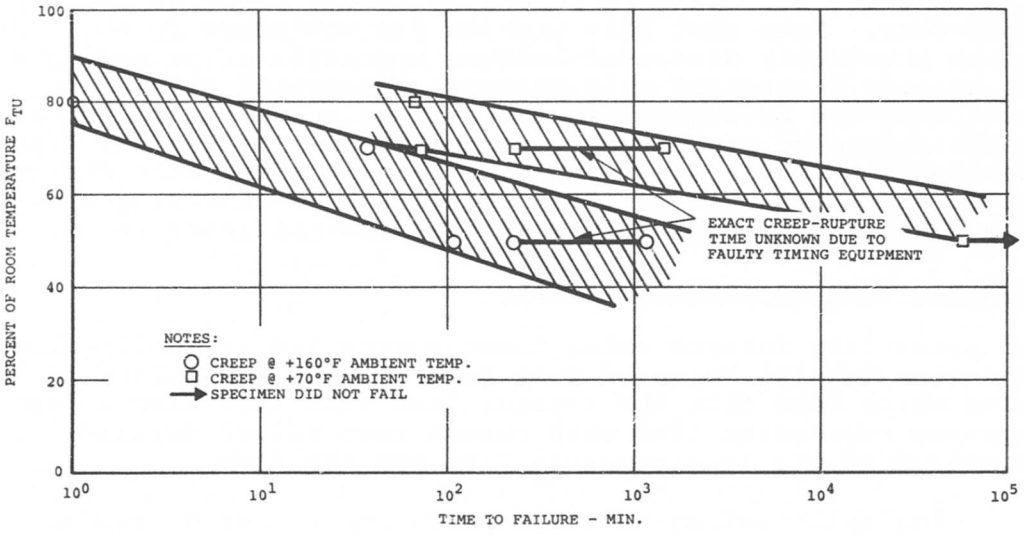

Figure 16. Unidirectional, 0°, S-Glass Laminate Creep Rupture Test Results.

deviation and coefficient of variation are calculated. It is assumed that the coefficient of variation remains constant and that the standard deviation varies according to the equation

$$\sigma_n = \text{(coefficient of variation)} * \text{(mean of test points at n cycles)}$$

The line labeled "Test Mean -3σ" is calculated by subtracting three standard deviations from each ordinate of the "Mean of Test Data" curve. The line labeled "Design Allowable Curve" is obtained by dividing each ordinate of the "Test Mean -3σ" curve between 10^5 and 10^8 cycles by 1.75. The 1.75 factor is the currently established value used to relate coupon tests with the expected performance of full-scale composite components in a long-time service environment.

The mixed-modulus and ±45° graphite laminate fatigue data, obtained by utilizing a Sonntag SF-10 fatigue machine (Figure 17), are presented in Tables VI and VII while the S-N curves are presented in Figures 18 and 19, respectively. Figure 20 presents the mean of the S-N data curves for the mixed-modulus laminates and its components. An S-N comparison of ±45° graphite with ±45° boron and ±45° S-glass is shown in Figure 21. Figure 22 presents comparative failure modes for the various tests performed on the ±45° graphite laminates. The failure mode for the mixed-modulus fatigue laminates is relatively the same as for the static results of Figure 6, but only if the alternating stress (of Figure 18) is below approximately 21 KSI. If the alternating stress is above 21 KSI, then the failure mode is one of premature failure of the graphite angle-ply near the doubler, resulting in the specimen's slipping out from between the doublers. Note that the grips were of the bolted variety and that the same problems occurred at the higher loads as occurred in the creep tests.

TUBE FABRICATION

The tubular specimens were fabricated in a single cure cycle using the parameters of Figure 2. Both sets of mixed-modulus and ±45° graphite tubes used the internal expanding mandrel technique described in Figures 23, 24 and 25. The mixed-modulus tubes were cured in an autoclave (using Figure 2) after the aluminum mold was assembled, wrapped with a bleeder cloth, and vacuum bagged. However, the ±45° graphite tubes used a different curing method to eliminate dependence on the autoclave and bag integrity for the maintenance of external pressure on the mold (used for safety purposes). These tubes were cured by placing the mold in a press to achieve clamping pressure while a bottled nitrogen source was used for internal mandrel pressure. The application of heat through the press platens and the new system of pressure application were found to be entirely satisfactory.

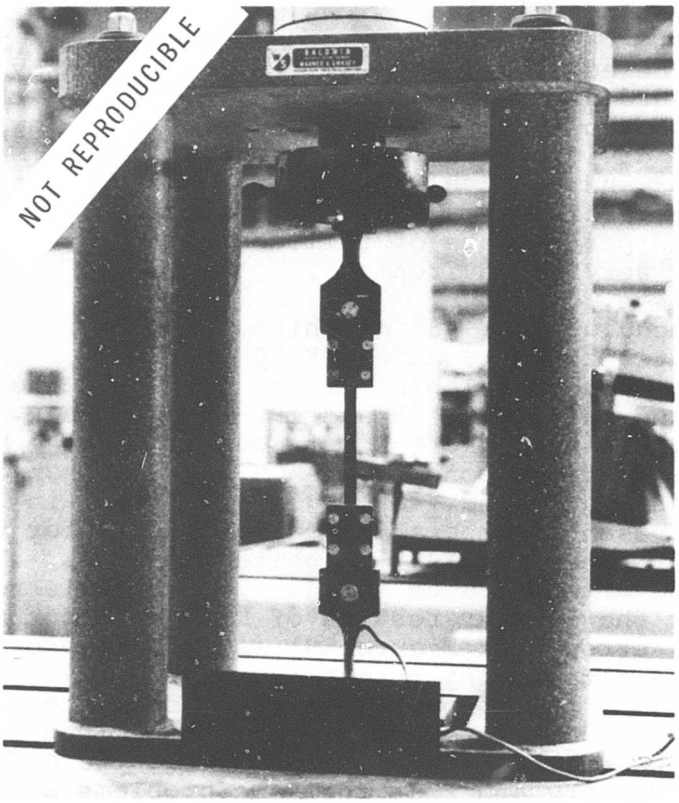

Figure 17. Laminate Tension-Tension Fatigue Test Setup.

TABLE VI. MIXED-MODULUS LAMINATE FATIGUE TEST RESULTS

SPECIMEN NUMBER	SPECIMEN WIDTH (IN.)	SPECIMEN THICKNESS (IN.)	SPECIMEN AREA ($IN.^2$)	ALTERNATING LOAD (LBS)	ALTERNATING STRESS (R=0.10) (PSI)	CYCLES TO FAILURE ($x10^{-6}$)	LOCATION OF FAILURE ORIGIN
1	.5003	.1350	.0675	2020	30000	.005	Doubler
2	.5007	.1382	.0692	2075	30000	.009	Doubler
6	.5004	.1390	.0696	1740	25000	.027	Doubler
7	.5000	.1370	.0685	1710	25000	.026	Doubler
8	.5004	.1334	.0668	1330	20000	.475	Doubler
9	.5005	.1180	.0591	1180	20000	.043	Doubler
10	.5000	.1360	.0680	1222	18000	5.446	Doubler
11	.5002	.1270	.0635	1460	23000	.032	Doubler
12	.5006	.1370	.0686	1310	19000	3.313	Doubler
13	.5003	.1390	.0695	1460	21000	.190	Doubler
14	.5005	.1382	.0690	1520	22000	.052	Doubler
15	.5005	.1377	.0690	1930	28000	.003	Doubler
16	.5007	.1385	.0693	1840	26500	.006	Doubler
17	.5000	.1372	.0686	1335	19500	3.391	Doubler
18	.5008	.1385	.0694	1350	19500	.984	Doubler

TABLE VII. ±45° GRAPHITE LAMINATE FATIGUE TEST RESULTS

SPECIMEN NUMBER	SPECIMEN WIDTH (IN.)	SPECIMEN THICKNESS (IN.)	SPECIMEN AREA ($IN.^2$)	ALTERNATING LOAD (LBS)	ALTERNATING STRESS (R=0.10) (PSI)	CYCLES TO FAILURE ($x10^{-6}$)	LOCATION OF FAILURE ORIGIN
GF-1*	.5005	.0417	.0209	62.5	3000	4.824	No Failure
				73.0	3500	12.369	No Failure
				83.0	4000	6.518	No Failure
				93.5	4500	2.564	No Failure
				104	5000	2.343	No Failure
				115	5500	2.214	No Failure
				125	6000	.364	Test Section
GF-2	.4999	.0439	.0219	131	6000	.199	Test Section
GF-3	.4995	.0476	.0238	Actual Load Unknown			
GF-4	.5005	.0466	.0233	135	5800	.168	Test Section
GF-5	.5007	.0457	.0229	129	5600	.893	Test Section
GF-6	.4996	.0466	.0233	126	5400	.213	Test Section
GF-7	.5002	.0439	.0220	114	5200	6.522	Test Section
GF-8	.4993	.0448	.0224	114	5100	5.808	Test Section
GF-9	.5001	.0439	.0220	112	5100	6.333	Test Section
GF-10	.4989	.0453	.0226	133	5900	<.001	Test Section
GF-11	.4996	.0419	.0209	Incorrect Stress Ratio			
GF-12	.4997	.0462	.0231	141	6100	.006	Test Section
GF-13	.5003	.0399	.0200	122	6100	.473	Test Section
GF-14	.4996	.0476	.0238	143	6000	.004	Test Section

*GF-1 was used to locate the failure region on an S-N plot. The value, however, was not plotted in Figure 19.

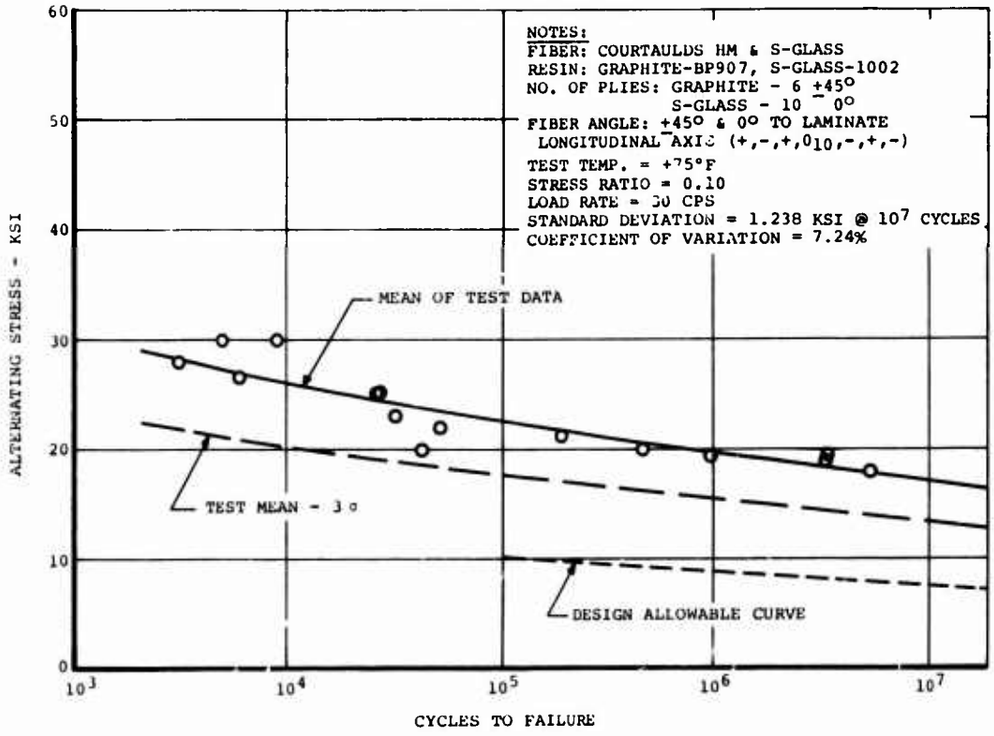

Figure 18. S-N Curve for Mixed-Modulus Tensile Laminates.

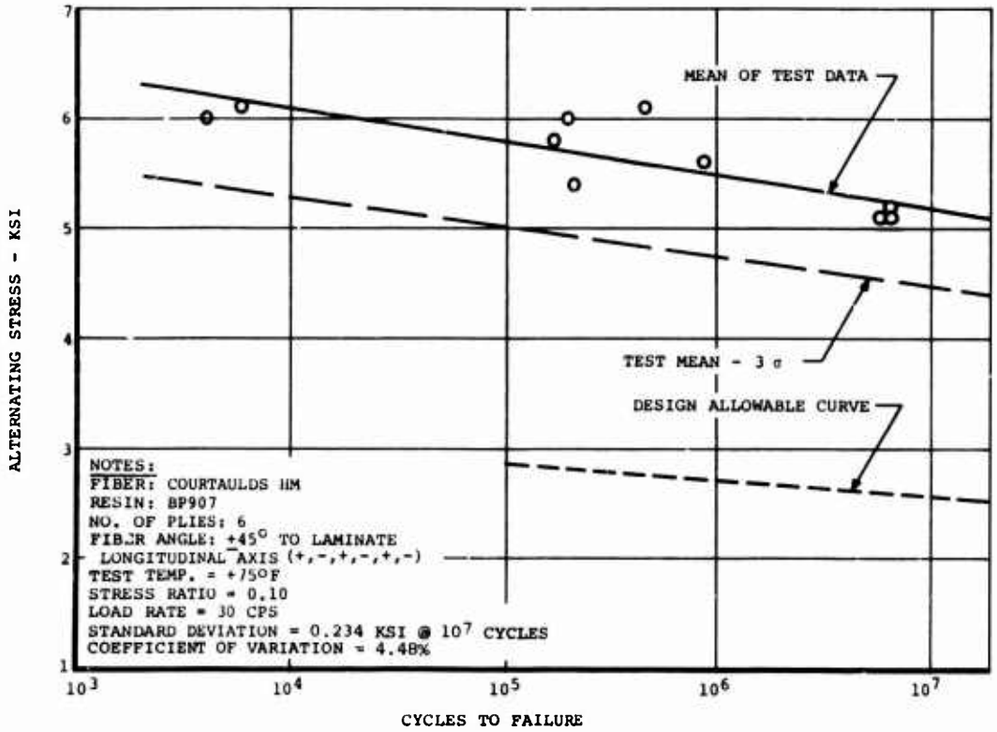

Figure 19. S-N Curve for ±45° Graphite Tensile Laminates.

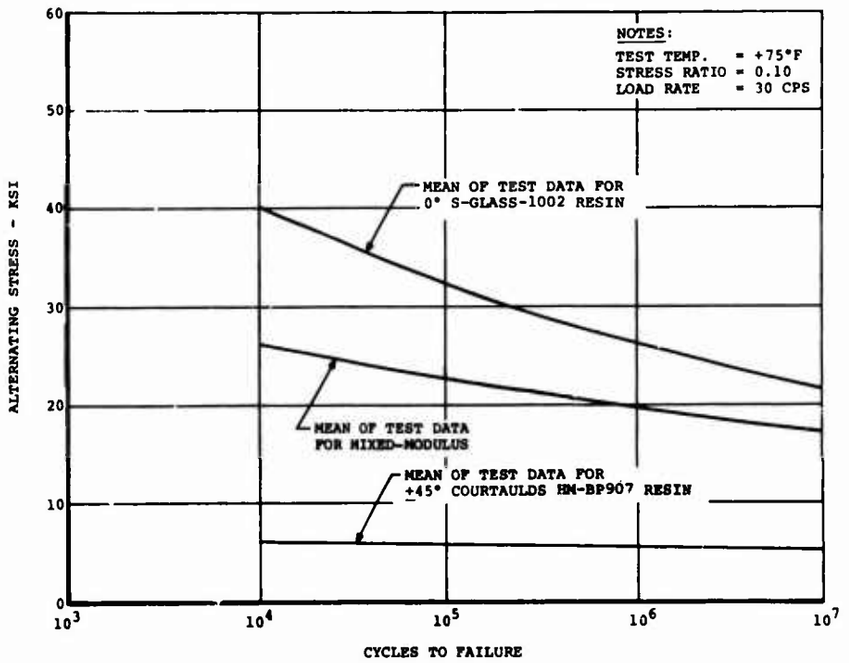

Figure 20. S-N Comparison of Mixed-Modulus, ±45° Graphite, and 0° S-Glass Tensile Laminates.

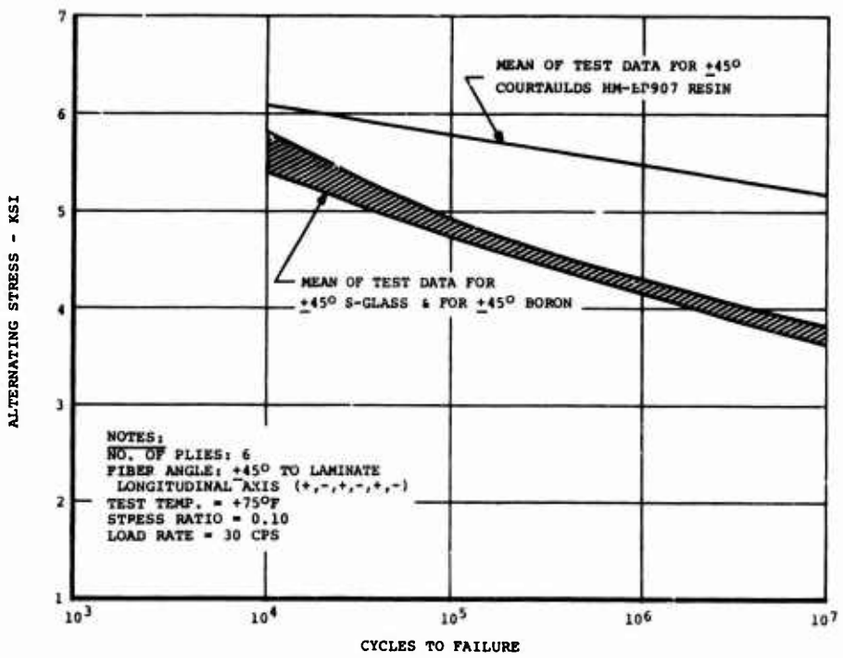

Figure 21. S-N Comparison of ±45° Graphite, S-Glass, and Boron Tensile Laminates.

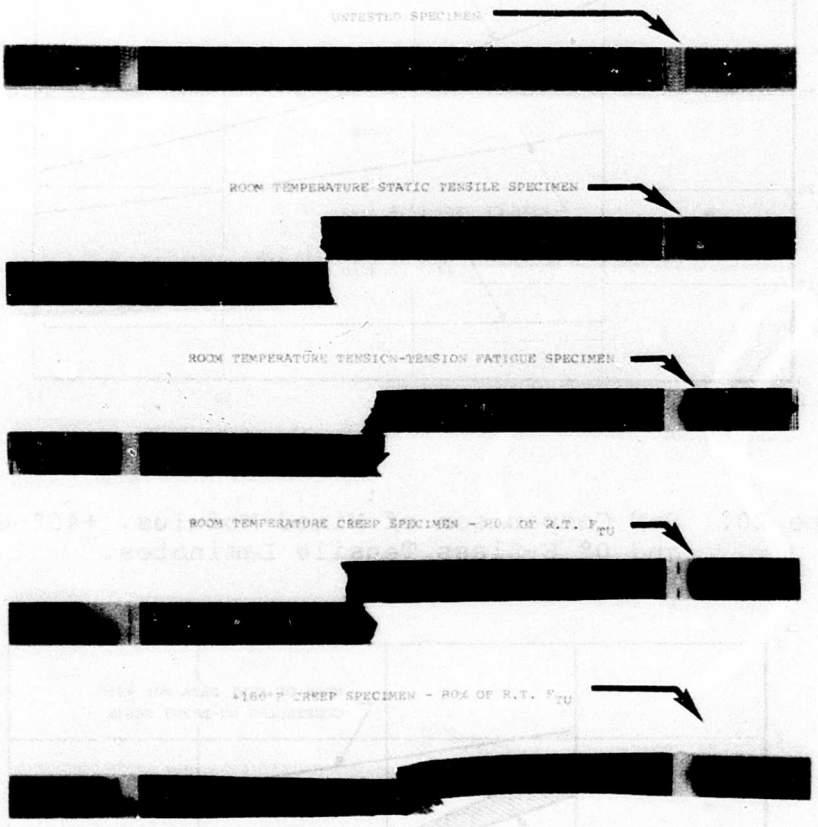

Figure 22. Comparative Failure Modes for the ±45° Graphite Laminates.

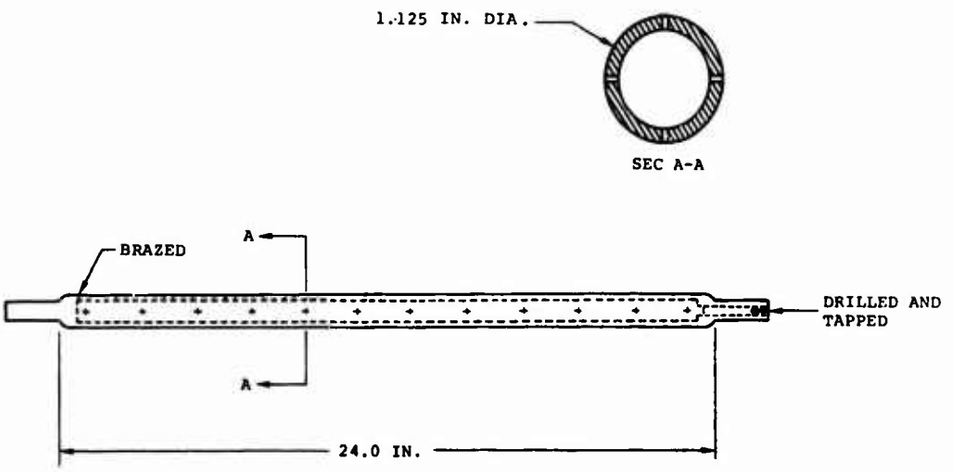

MATERIAL: 0.062 IN. WALL 2024-T3 ALUM TUBE - 2024-T3 ALUM ROUND STOCK BRAZED ON ENDS OF TUBE AND TURNED DOWN TO SIZE

Figure 23. Mandrel for 1.5-Inch Tubing Mold.

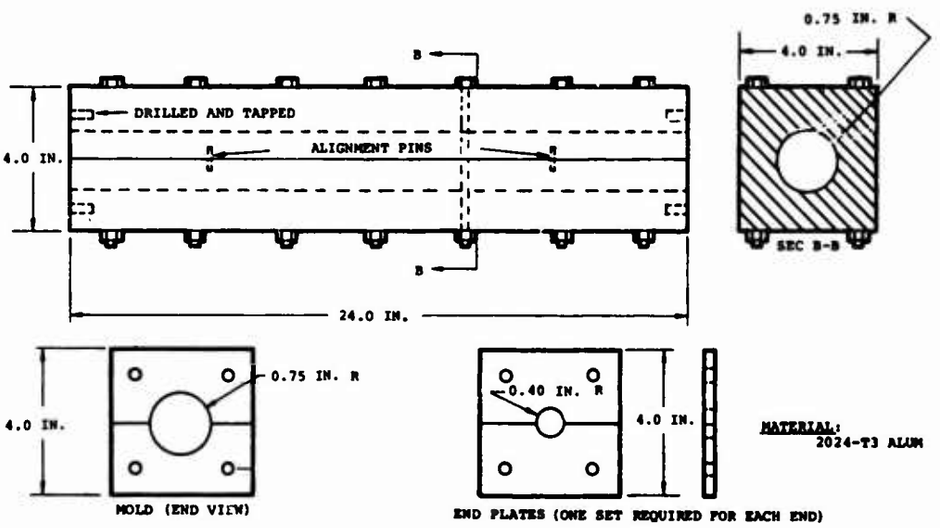

Figure 24. Tubing Mold.

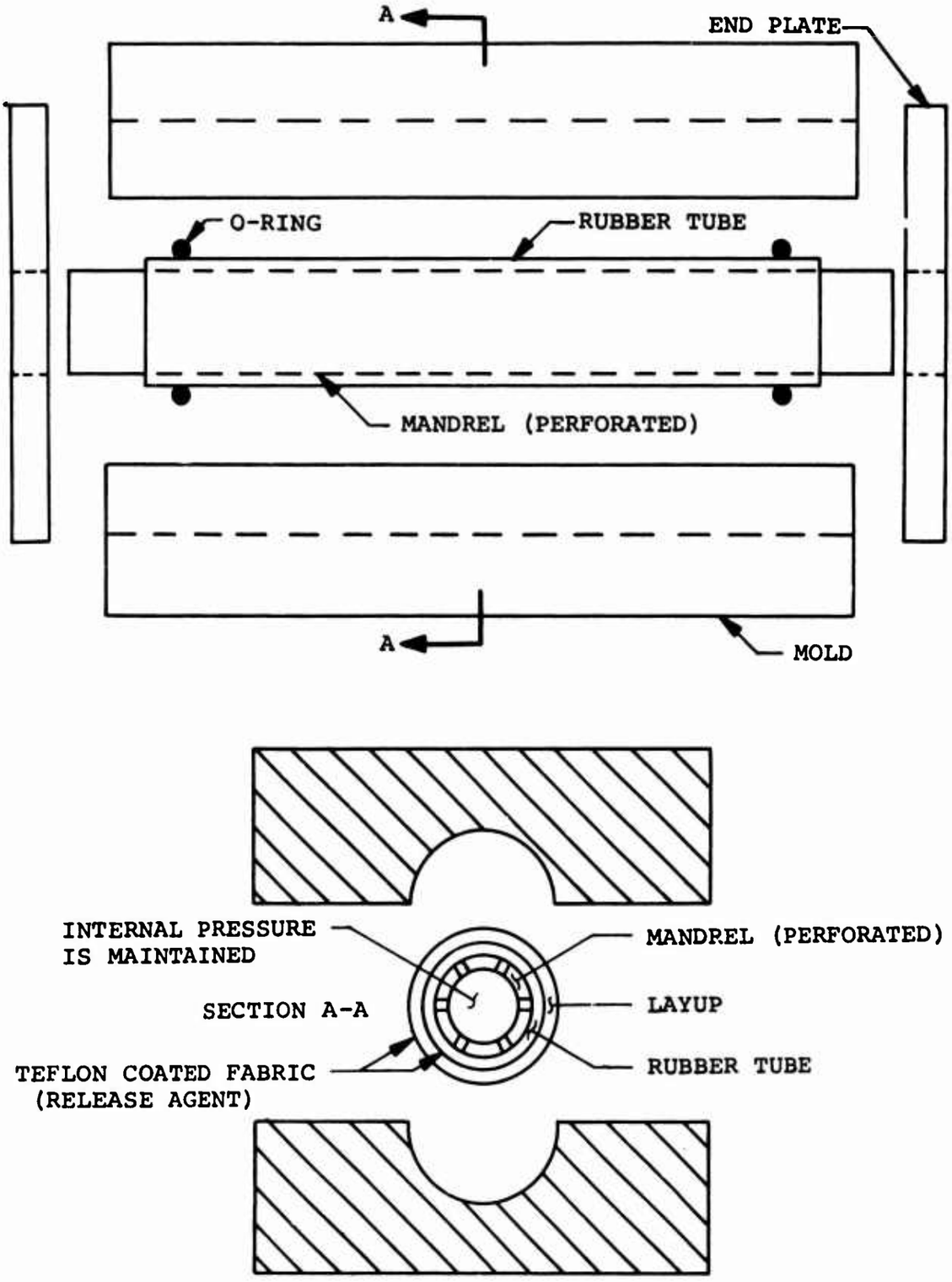

Figure 25. Torsion Tube Specimen Tooling.

All the mixed-modulus and the static graphite tubes had doublers, consisting of 181 S-glass cloth oriented at ±45° to the tube longitudinal axis subsequently bonded on, while the ±45° graphite fatigue tubes had no doublers applied but instead had an aluminum plug (1 inch long) bonded into each end of the specimens.

TUBE TESTING

Static Shear Tests

Static testing of the mixed-modulus and the ±45° graphite tubes yielded the results presented in Tables VIII and IX, respectively, along with the typical shear stress versus angle of twist curves for the mixed-modulus and its constituent materials, shown in Figure 26. The tests were conducted in the 120-kip Baldwin test machine utilizing a torsion test fixture schematically presented in Figures 27 and 28, with Figure 29 showing the actual test setup. The aluminum end caps which were bonded to the specimen (Figure 27) were bolted to the two wheels of a jig (Figure 28). Torque was applied to the specimen as the wheels were rotated relative to one another by cables wrapped around the circumference of the wheels and loaded by the test machine through an evener system. A displacement transducer was adapted to measure the angle of twist over a 2.50-inch gage length while the test machine was set to twist the specimen at a constant rate equivalent to 0.003 radian/minute.

From Figure 26, it is seen that as the mixed-modulus tube is loaded, the shear strain limit of the ±45° angle-ply graphite is reached, causing it to fail. However, total failure was avoided because of the geometrical effect, where the cracked graphite layers, which were not sheared from the 0° S-glass, "relock" themselves and transmit part of the applied torque through bearing loads along the cracks. This phenomenon suggests that a satisfactory interface bond existed between the two resin systems (i.e., between the BP907 and the 1002). Figure 30 presents typical failed static tube specimens.

Dynamic Torsion Testing

The mixed-modulus testing was done on the Baldwin SF-1U fatigue machine, and the ±45°graphite tubes were tested on the SF-1 Sonntag test unit (Figure 31). Tables X and XI present the corresponding fatigue data, while Figures 32 and 33 describe the resulting S-N curves. Figure 34 presents the mean of the S-N data curves for the mixed-modulus tubes and its constituent materials. An S-N comparison of ±45° graphite torsion tubes with ±45° S-glass tubes is shown in Figure 35. Figure 36 presents typical dynamic failure modes for the ±45° graphite tubes which are similar for the static specimens, while the failure modes for the mixed-modulus tubes were similar to those presented in Figure 30.

TABLE VIII. MIXED-MODULUS TORSION TUBE STATIC TEST RESULTS

SPECIMEN NUMBER	AVERAGE OUTSIDE DIAMETER D_o-(IN.)	AVERAGE INSIDE DIAMETER D_i-(IN.)	AVERAGE WALL THICKNESS t-(IN.)	POLAR MOMENT OF INERTIA J-(IN.^{4})	ULTIMATE TORQUE T-(IN.-LBS)	ULTIMATE SHEAR STRESS τ-(PSI)*	SHEAR MODULUS G-(x10^{-6}PSI)	LOCATION OF FAILURE ORIGIN
2	1.500	1.386	.057	.1347	3348	17900	2.59	Test Section
3	1.502	1.384	.059	.1395	3492	18100	2.75	Test Section
4	1.500	1.374	.063	.1471	3462	16900	2.50	Test Section
5	1.502	1.377	.063	.1467	3558	17500	2.65	Test Section
6	1.500	1.380	.060	.1410	3762	19200	2.82	Test Section
					AVERAGE	17900	2.66	

* $\tau = \frac{Tc}{J}$, $c=(D_o-t)/2$

TABLE IX. ±45° GRAPHITE TORSION TUBE STATIC TEST RESULTS

SPECIMEN NUMBER	AVERAGE OUTSIDE DIAMETER (IN.)	AVERAGE INSIDE DIAMETER (IN.)	AVERAGE WALL THICKNESS (IN.)	POLAR MOMENT OF INERTIA (IN.^{4})	ULTIMATE TORQUE (IN.-LBS)	ULTIMATE SHEAR STRESS (PSI)	SHEAR MODULUS (x10^{-6}PSI)	LOCATION OF FAILURE ORIGIN
101	1.504	1.408	.048	.1165	4170	26100	4.58	Test Section
102	1.504	1.404	.050	.1209	4224	25400	4.37	Test Section
103	1.500	1.399	.051	.1209	4206	25200	4.16	Test Section
104	1.501	1.401	.050	.1201	4326	26100	4.37	Test Section
105	1.501	1.410	.046	.1103	3906	25800	4.89	Test Section
					AVERAGE	25700	4.47	

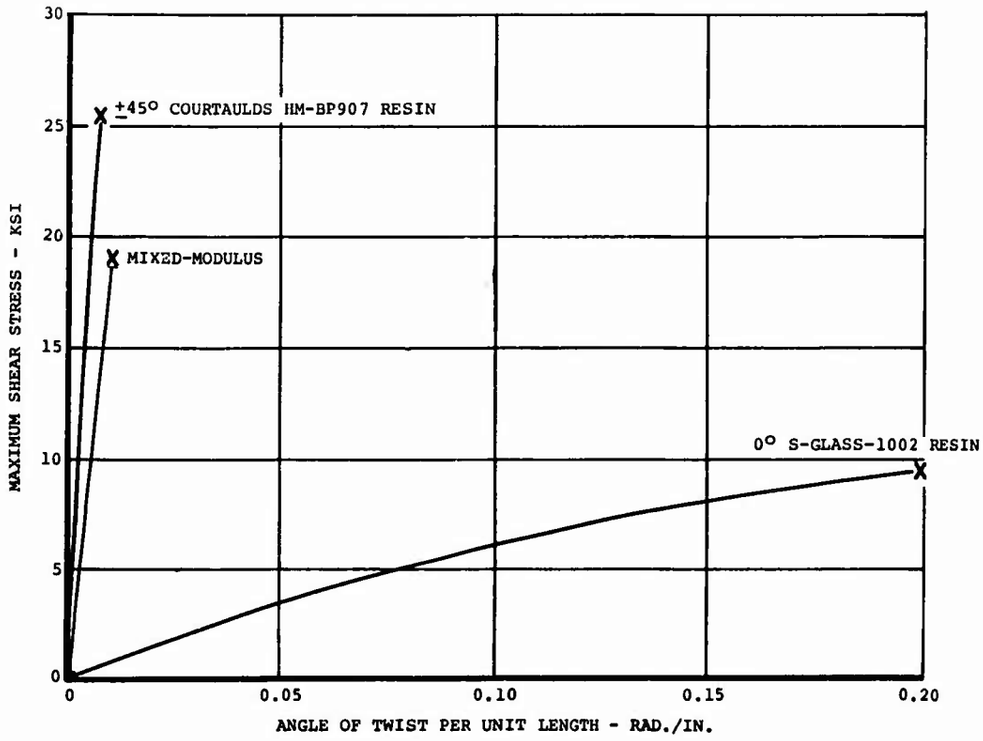

Figure 26. Typical Shear Stress-Angle of Twist Curve for Torsion Tube Specimens.

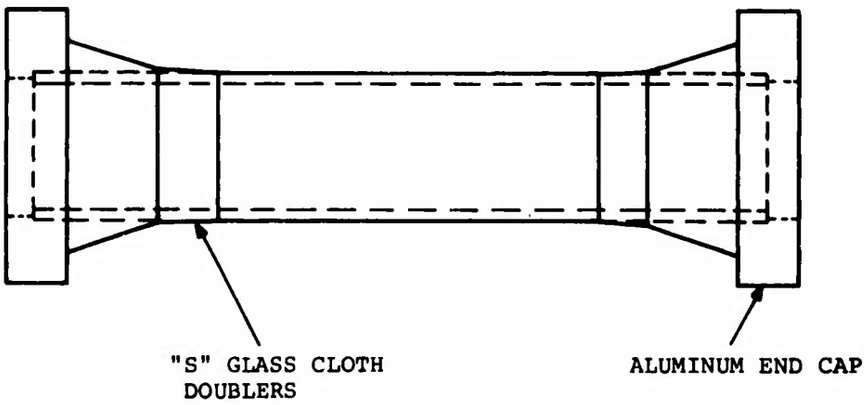

Figure 27. Static Torsion Tube Test Specimen.

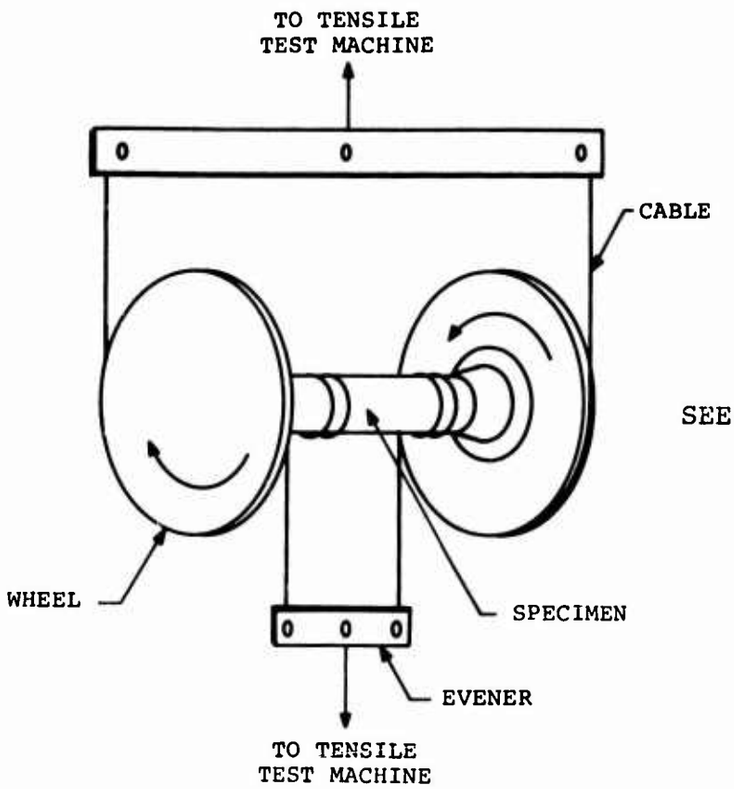

Figure 28. Static Torsion Tube Test Fixture.

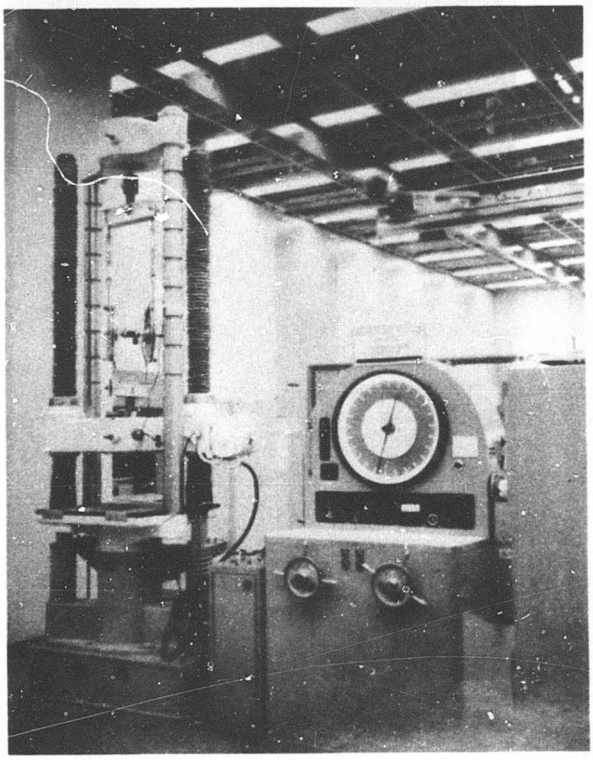

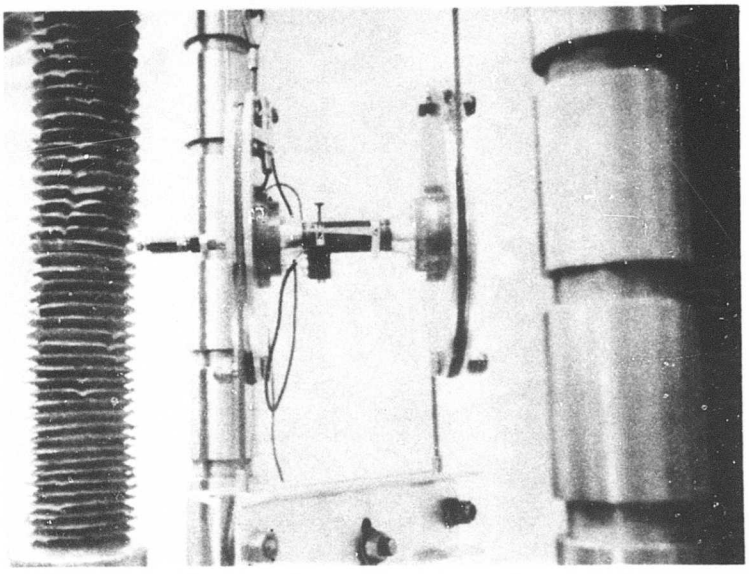

Figure 29. Static Torsion Tube Test Setup.

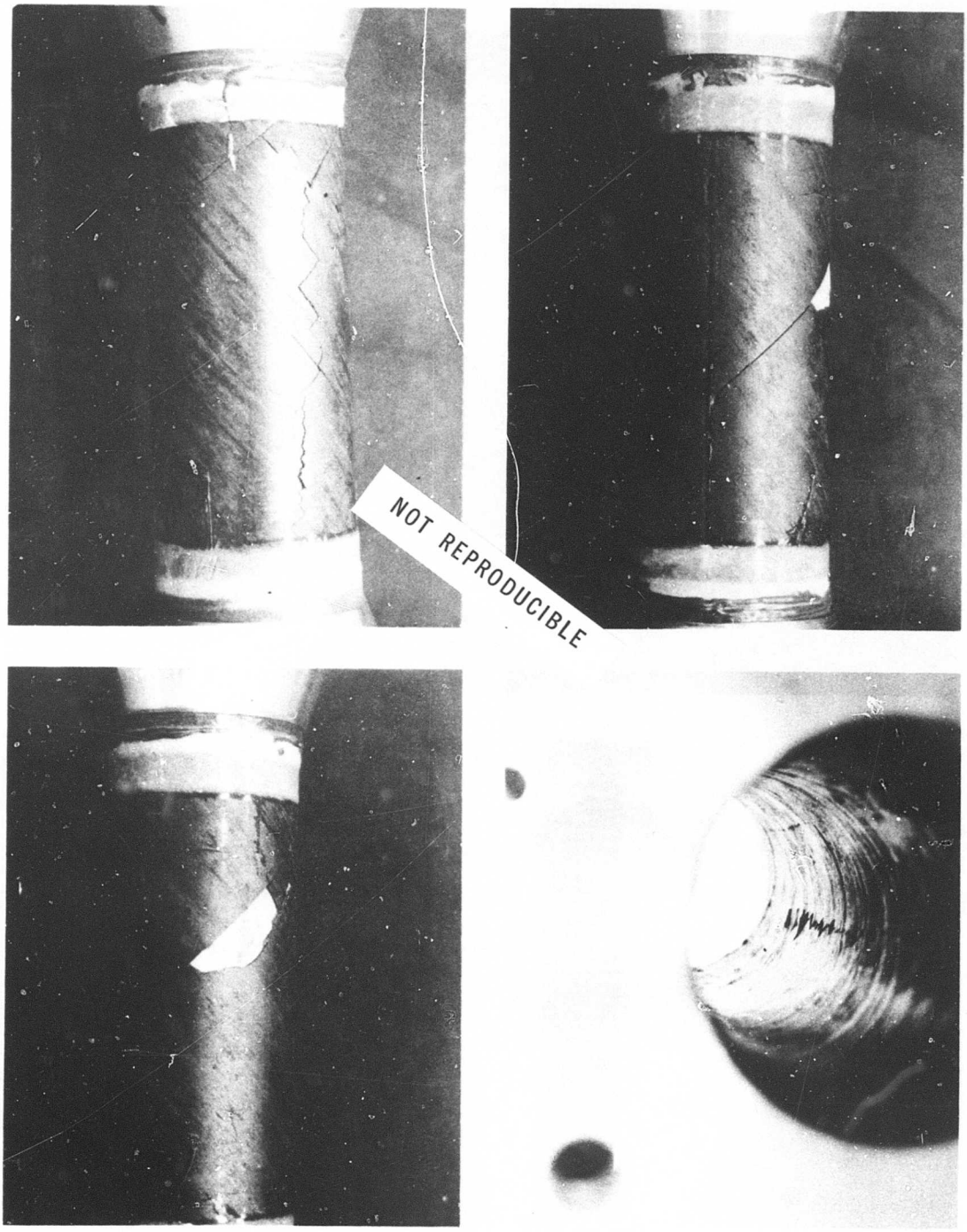

Figure 30. Typical Failed Mixed-Modulus Static Torsion Tube Specimens.

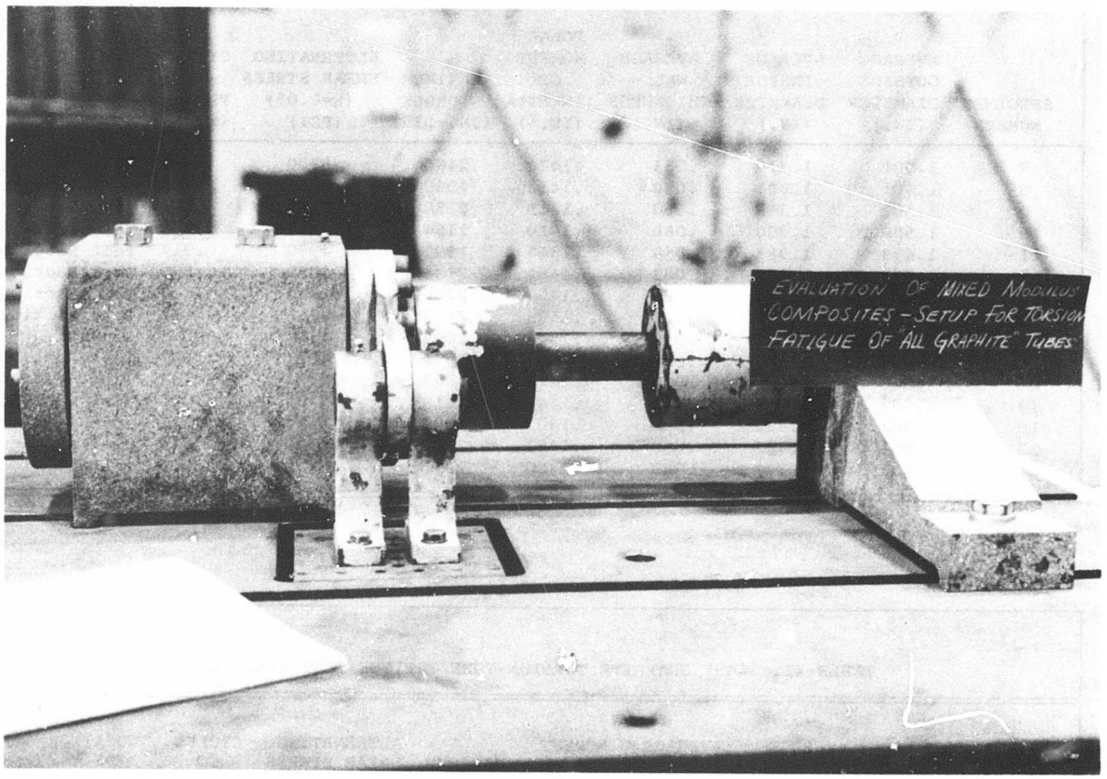

Figure 31. Torsion Tube Fatigue Test Setup.

TABLE X. MIXED-MODULUS TORSION TUBE FATIGUE TEST RESULTS

SPECIMEN NUMBER	AVERAGE OUTSIDE DIAMETER (IN.)	AVERAGE INSIDE DIAMETER (IN.)	AVERAGE WALL THICKNESS (IN.)	POLAR MOMENT OF INERTIA ($IN.^4$)	MAXIMUM TORQUE (IN.-LBS)	ALTERNATING SHEAR STRESS (R=0.05) (PSI)	CYCLES TO FAILURE ($x10^{-6}$)	LOCATION OF FAILURE ORIGIN
7	1.501	1.375	.063	.1474	2460	5700	.025	Test Section
8	1.501	1.381	.060	.1412	1960	4750	2.601	Test Section
9	1.502	1.382	.060	.1415	2158	5220	.102	Test Section
10	1.500	1.380	.060	.1410	2154	5220	.035	Test Section
11	1.499	1.383	.058	.1365	1990	4990	.917	Test Section
12	1.500	1.375	.063	.1461	2134	4980	.529	Test Section
13	1.498	1.378	.060	.1404	2246	5460	.126	Test Section
14	1.504	1.370	.067	.1565	2177	4750	.513	Test Section
15	1.502	1.386	.058	.1374	1808	4510	19.066	Runout
16	1.500	1.379	.061	.1420	1874	4510	2.002	Test Section
17	1.500	1.380	.060	.1410	1802	4370	2.761	Test Section
18	1.502	1.379	.062	.1446	2410	5700	.085	Test Section
19	1.502	1.383	.060	.1405	2299	5600	.214	Test Section
20	1.501	1.382	.060	.1402	2411	5890	.014	Test Section
21	1.503	1.377	.063	.1480	2631	6080	.009	Test Section

TABLE XI. $\pm 45°$ GRAPHITE TORSION TUBE FATIGUE TEST RESULTS

SPECIMEN NUMBER	AVERAGE OUTSIDE DIAMETER (IN.)	AVERAGE INSIDE DIAMETER (IN.)	AVERAGE WALL THICKNESS (IN.)	POLAR MOMENT OF INERTIA ($IN.^4$)	MAXIMUM TORQUE (IN.-LBS)	ALTERNATING SHEAR STRESS (R=0.10) (PSI)	CYCLES TO FAILURE ($x10^{-6}$)	LOCATION OF FAILURE ORIGIN
GTF 1	1.502	1.405	.049	.1171	3320	9270	Failed on Start	
GTF 2	1.502	1.405	.049	.1171	1959	5470	6.890	No Failure
					2360	6590	.284	Test Section
GTF 3	1.500	1.408	.016	.1111	2222	6540	Failed on Installation	
GTF 4	1.506	1.408	.049	.1192	2413	6640	15.509	No Failure
					2622	7210	5.016	No Failure
					2815	7740	1.286	Test Section
GTF 5	1.509	1.406	.052	.1254	2923	7640	2.619	Test Section
GTF 6	1.505	1.406	.052	.1200	3131	8530	11.982	Test Section
GTF 7	1.502	1.410	.046	.1116	2980	8750	16.588	No Failure
					3145	9230	1.367	Test Section
GTF 8	1.502	1.406	.048	.1160	3252	9170	.073	Under Clamp
GTF 9	1.504	1.408	.048	.1165	3293	9260	.097	Test Section
GTF 10	1.505	1.409	.048	.1167	3887	10920	.002	Test Section
GTF 11	1.509	1.409	.050	.1221	3560	9570	Failed on Installation	
GTF 12	1.503	1.410	.047	.1129	3560	10330	Failed on Start	
GTF 13	1.505	1.413	.046	.1123	3268	9550	.002	Test Section
GTF 14	1.502	1.406	.048	.1160	3018	8510	.013	At Clamp
GTF 15	1.504	1.408	.048	.1165	2968	8350	Failed on Start	

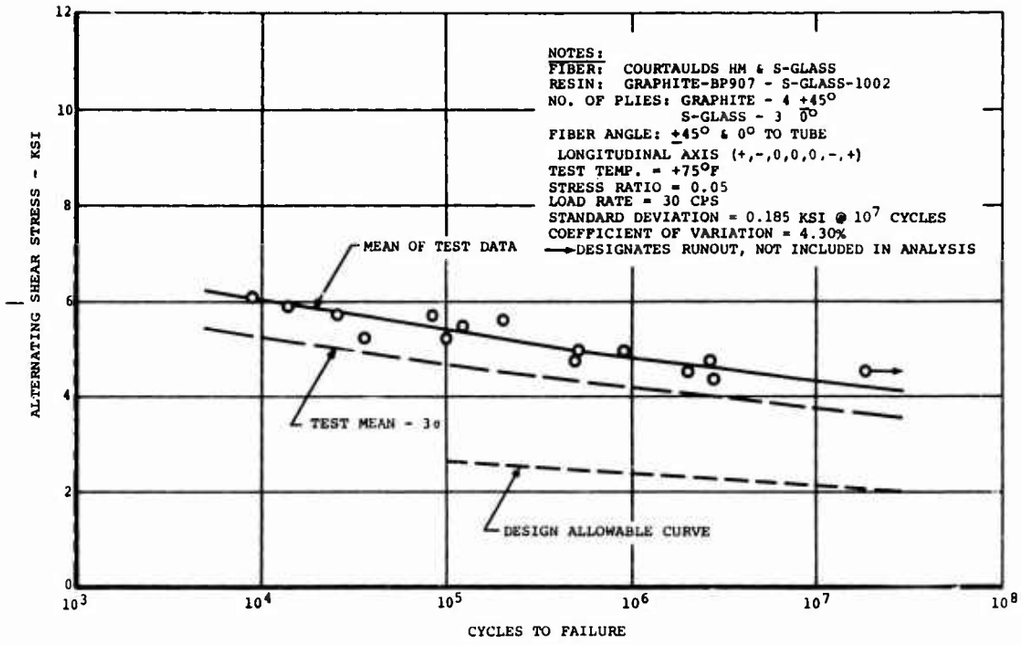

Figure 32. S-N Curve for Mixed-Modulus Torsion Tubes.

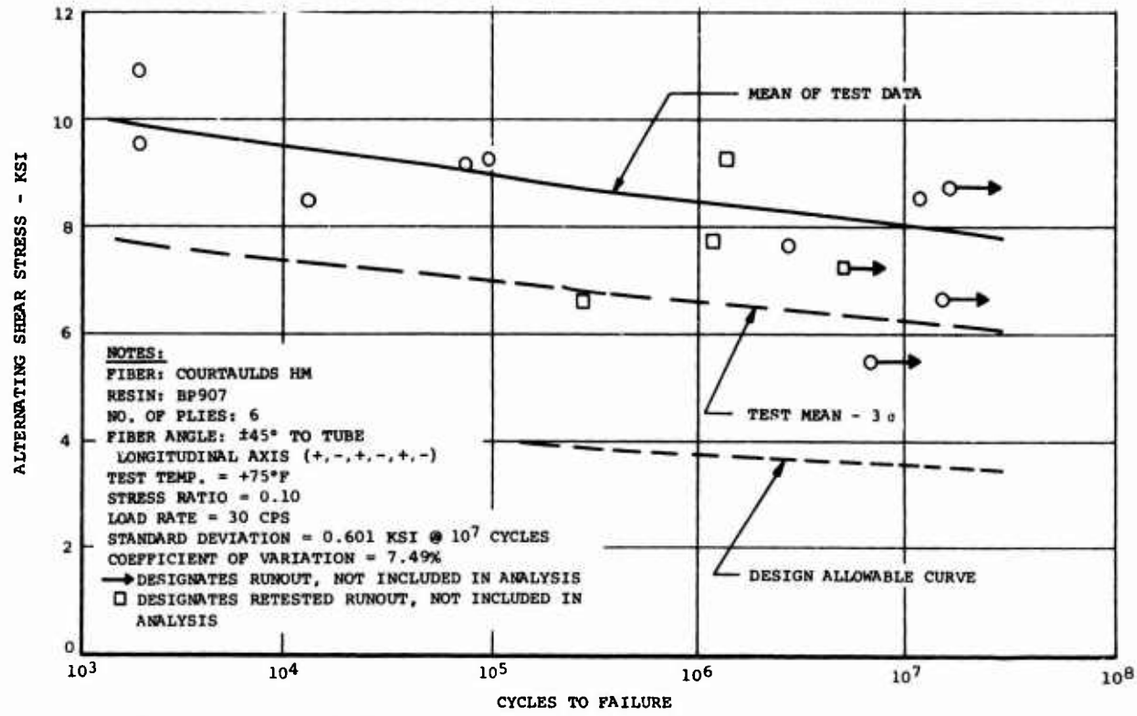

Figure 33. S-N Curve for ±45° Graphite Torsion Tubes.

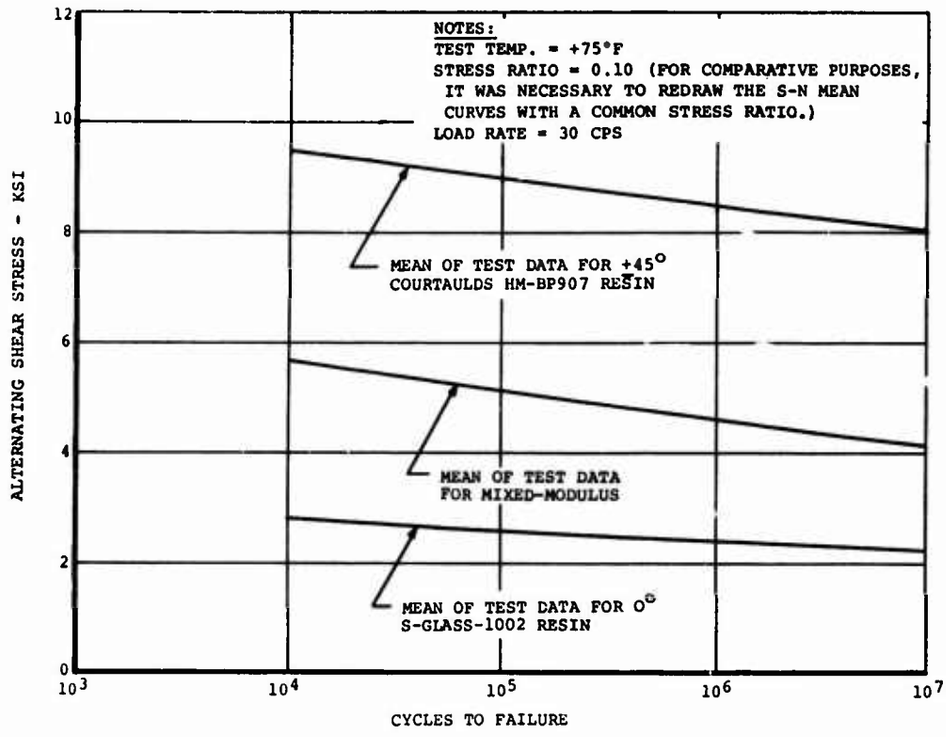

Figure 34. S-N Comparison of Mixed-Modulus, +45° Graphite, and 0° S-Glass Torsion Tubes.

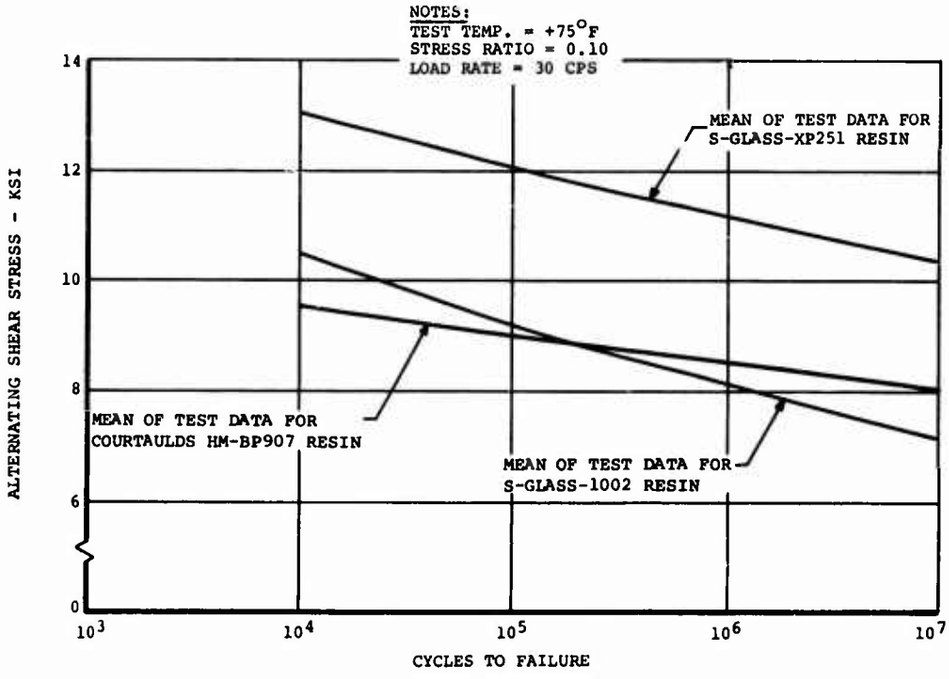

Figure 35. S-N Comparison of ±45° S-Glass and Graphite Torsion Tubes.

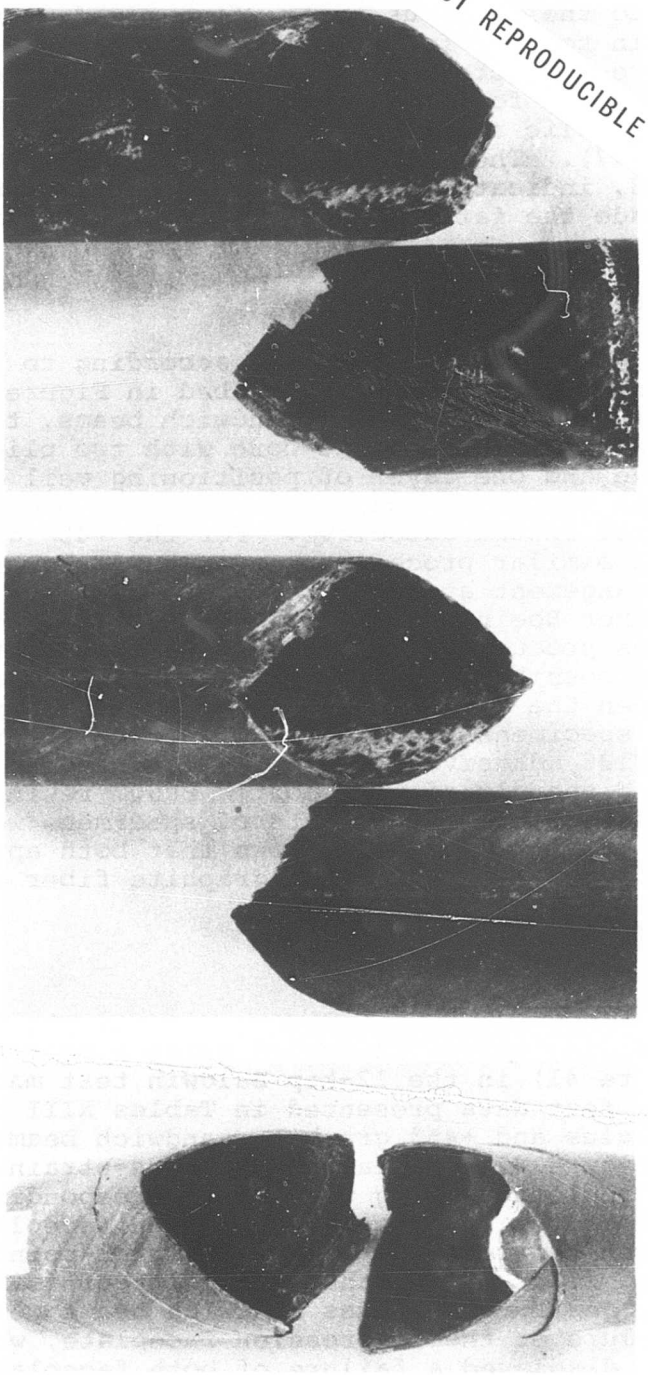

Figure 36. Typical Failed ±45° Graphite Dynamic Torsion Tube Specimens.

In addition to the previous tests, five mixed-modulus tubes were tested in torsion fatigue with a constant axial loading. The tests were conducted in the same test apparatus as the pure torsion tests for the mixed-modulus tubes with the addition of a hydraulic actuator and hand pump to apply the axial load (Figure 37). The test results, presented in Table XII and Figure 38, indicate that the steady tensile load apparently did not degrade the fatigue performance of the mixed-modulus tube.

SANDWICH FABRICATION

The sandwich panels were fabricated according to Figure 39 utilizing a single-stage cure described in Figure 2. In such a process for the mixed-modulus sandwich beams, the skins were laid up and positioned onto the core with two plies of 5-mil AF126 adhesive and one layer of positioning veil at each bondline, and then the whole assembly was vacuum bagged on a caul plate and cured in the autoclave. For the $\pm 45°$ graphite sandwich beams, a similar procedure was followed, except for a different arrangement at the core/skin bond line. It had been noted from other Boeing testing that a single-stage cure using graphite skins produced severe skin dimpling and fiber damage. To avoid this possibility, the effects of two different scrim systems between the skin and the core were investigated. The first set of specimens had one ply of BP907-120 prepreg and one ply of AF126 adhesive between the core and skin, while the second set had one ply of unsupported BP907 resin and one ply of dry 104 glass cloth. Both sets of specimens were bagged and cured as usual. Figure 40 shows that both approaches proved satisfactory in preventing graphite fiber damage.

SANDWICH TESTING

Static Bending Tests

The static bending tests, conducted using a four-point loading fixture (Figure 41) in the 12-kip Baldwin test machine, resulted in the test data presented in Tables XIII and XIV for the mixed-modulus and $\pm 45°$ graphite sandwich beams, respectively. In Figure 42, the laminate stress-strain curves of Figure 5 are replotted along with the corresponding stress-strain curves of the sandwich beam tension faceplate (which are calculated from the recorded specimen center-point deflection versus applied load). Note that the point of failure for the mixed-modulus and the $0°$ S-glass sandwich beams were characterized by a failure of the compression faceplate, while the $\pm 45°$ graphite beam displayed a failure of both faceplates. The failure pattern for the mixed-modulus sandwich beams, shown in Figure 43, apparently resulted from an induced tensile stress at $90°$ to the uni glass fibers (due to the influence of the aluminum honeycomb and the Poisson's effect) which caused

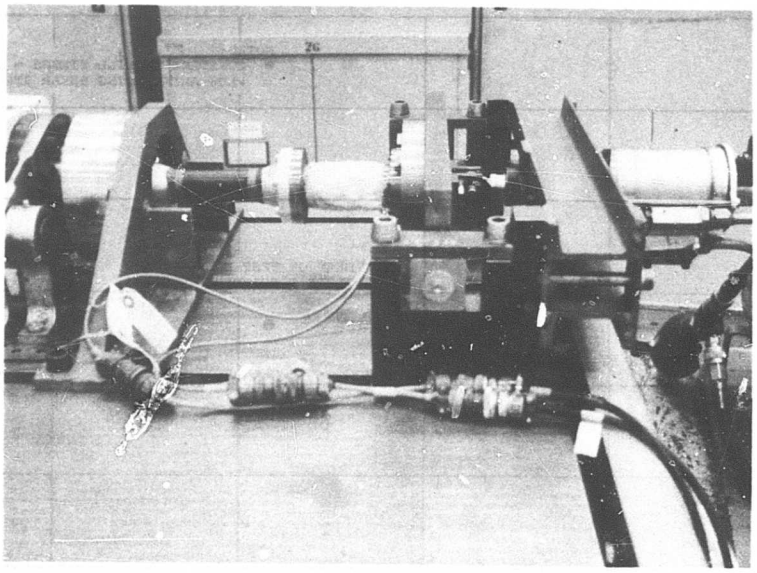

Figure 37. Torsion Tube Fatigue With Constant Axial Load Test Setup.

TABLE XII. MIXED-MODULUS TORSION TUBE FATIGUE TEST RESULTS (WITH A CONSTANT AXIAL TENSILE STRESS)

SPECIMEN NUMBER	AVERAGE OUTSIDE DIAMETER (IN.)	AVERAGE INSIDE DIAMETER (IN.)	AVERAGE WALL THICKNESS (IN.)	POLAR MOMENT OF INERTIA ($IN.^4$)	AXIAL TENSILE STRESS (PSI)	MAXIMUM TORQUE (IN.-LBS)	ALTERNATING SHEAR STRESS (R=0.05) (PSI)	CYCLES TO FAILURE ($x10^{-6}$)	LOCATION OF FAILURE ORIGIN
22	1.505	1.385	.060	.1424	18000	1577	3800	16.273	Runout
23	1.502	1.389	.057	.1342	18000	1856	4750	10.786	Runout
24	1.502	1.378	.062	.1457	18000	2428	5700	Failed on Start	
25	1.500	1.379	.061	.1420	18000	2169	5220	.695	Test Section
26	1.501	1.389	.056	.1329	18000	2098	5420	.282	Test Section

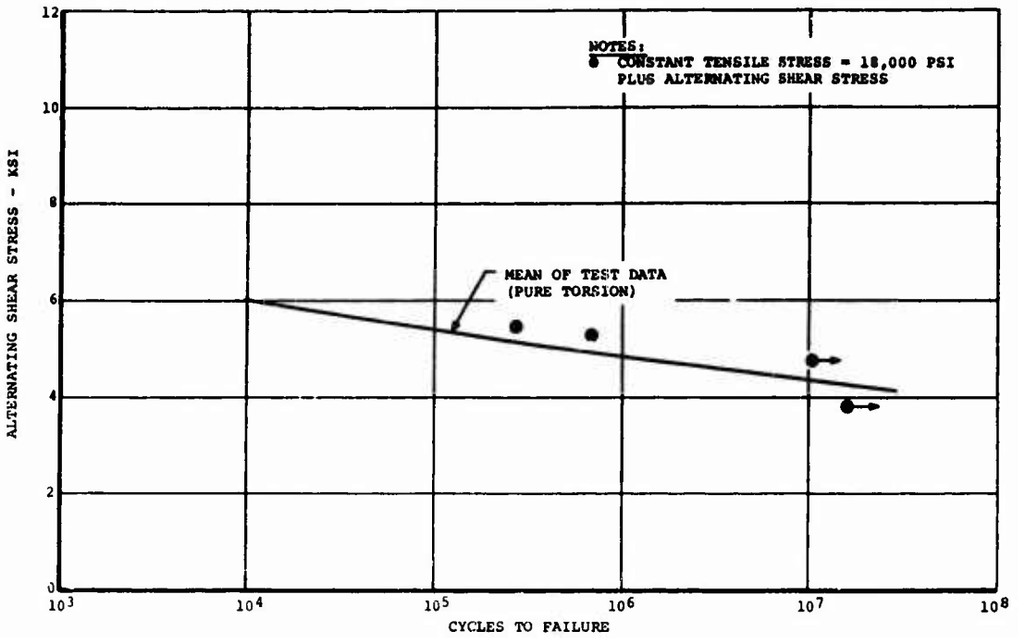

Figure 38. Effect of a Constant Tensile Stress on the S-N Curve for Mixed-Modulus Torsion Tubes.

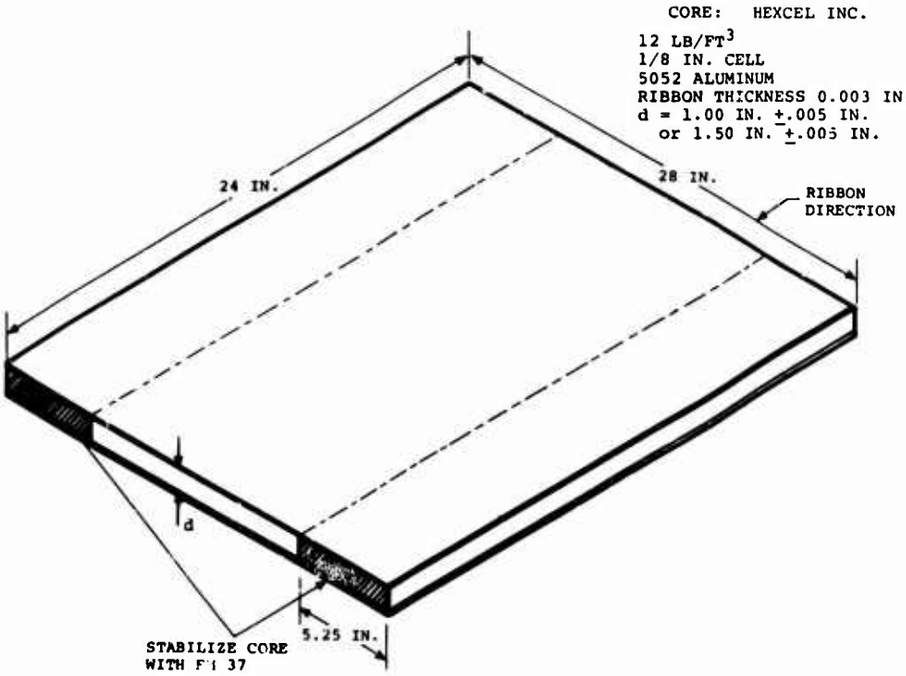

Figure 39. Sandwich Panel Construction.

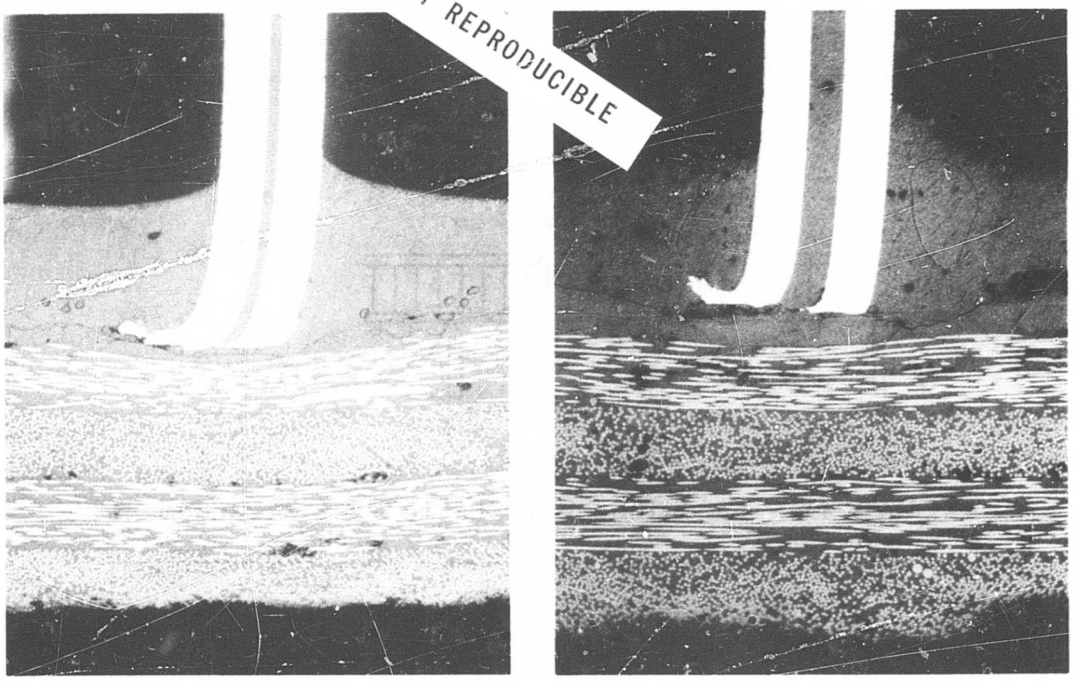

ADHESIVE BETWEEN FACEPLATES AND CORE

1 PLY BP907 UNSUPPORTED RESIN
1 PLY DRY 104 GLASS
1 PLY BP907-120 PREPREG
1 PLY AF126 ADHESIVE

Figure 40. Effectiveness of Scrim Cloth in Preventing Damage to Graphite Fibers.

TABLE XIII. MIXED-MODULUS SANDWICH BENDING BEAM STATIC TEST RESULTS

SPECIMEN NUMBER	SPECIMEN WIDTH b-(IN.)	SANDWICH THICKNESS d-(IN.)	CORE THICKNESS t_c-(IN.)	FACE-PLATE THICKNESS t-(IN.)	MOMENT OF INERTIA I-($IN.^4$)	ULTIMATE LOAD P-(LBS)	FACE-PLATE STRESS σ-(PSI)*	FACE-PLATE MODULUS E-($\times 10^{-6}$PSI)**	LOCATION OF FAILURE ORIGIN
1	1.805	1.068	1.001	.0334	.0324	1435	69000	5.15	Comp.Face
6	1.800	1.071	1.004	.0334	.0325	1400	67300	5.06	Comp.Face
13	1.808	1.068	1.001	.0334	.0324	1350	64800	5.17	Comp.Face
104	1.805	1.066	.999	.0334	.0322	1305	62900	5.14	Comp.Face
108	1.805	1.068	1.001	.0334	.0324	1445	69500	5.08	Comp.Face
					AVERAGE		66700	5.12	

* $\sigma = \dfrac{6P}{bt\ (d+t_c)}$

** $E = \dfrac{\Delta P}{\Delta Y}\ a_n\ \dfrac{(3L_n^2 - 4a_n^2)}{24I}$, $I = \dfrac{b}{12}\ (d^3 - t_c^3)$ $\dfrac{\Delta P}{\Delta Y}$: Slope of load-deflection curve

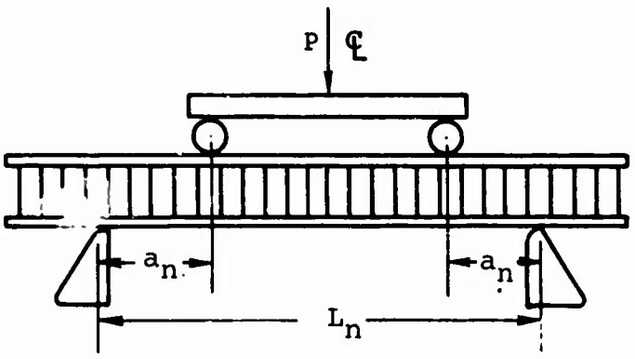

a_n = 6 in.

L_n = 16 in.

Figure 41. Sandwich Beam Static Test Arrangement.

TABLE XIV. ±45° GRAPHITE SANDWICH BENDING BEAM STATIC TEST RESULTS

SPECIMEN NUMBER		SPECIMEN WIDTH (IN.)	SANDWICH THICKNESS (IN.)	CORE THICKNESS (IN.)	FACE-PLATE THICKNESS (IN.)	MOMENT OF INERTIA ($IN.^4$)	ULTIMATE LOAD (LBS)	FACE-PLATE STRESS (PSI)	FACE-PLATE MODULUS ($\times 10^{-6}$PSI)	LOCATION OF FAILURE ORIGIN
US-1	*	1.998	1.565	1.504	.0306	.0718	924	29500	2.34	Ten. & Comp. Faces
US-2	*	1.998	1.564	1.503	.0306	.0717	940	30100	2.37	Ten. & Comp. Faces
US-3	*	1.997	1.564	1.503	.0306	.0716	944	30200	2.34	Ten. Face
						AVERAGE		29900	2.35	
PS-1	**	2.000	1.572	1.507	.0326	.0770	1150	34400	2.66	Ten. & Comp. Faces
PS-2	**	2.000	1.572	1.507	.0326	.0770	1115	33300	2.65	Ten. & Comp. Faces
PS-3	**	1.993	1.572	1.507	.0326	.0768	975	29200	2.60	Ten. & Comp. Faces
						AVERAGE		32300	2.64	

Adhesive between faceplates and core:

* - ±45° Graphite Faceplate
- 1 Ply BP907 Unsupported Resin
- 1 Ply Dry 104 Glass
- Aluminum Honeycomb Core

** - ±45° Graphite Faceplate
- 1 Ply BP907-120 Prepreg
- 1 Ply AF126 Adhesive
- Aluminum Honeycomb Core

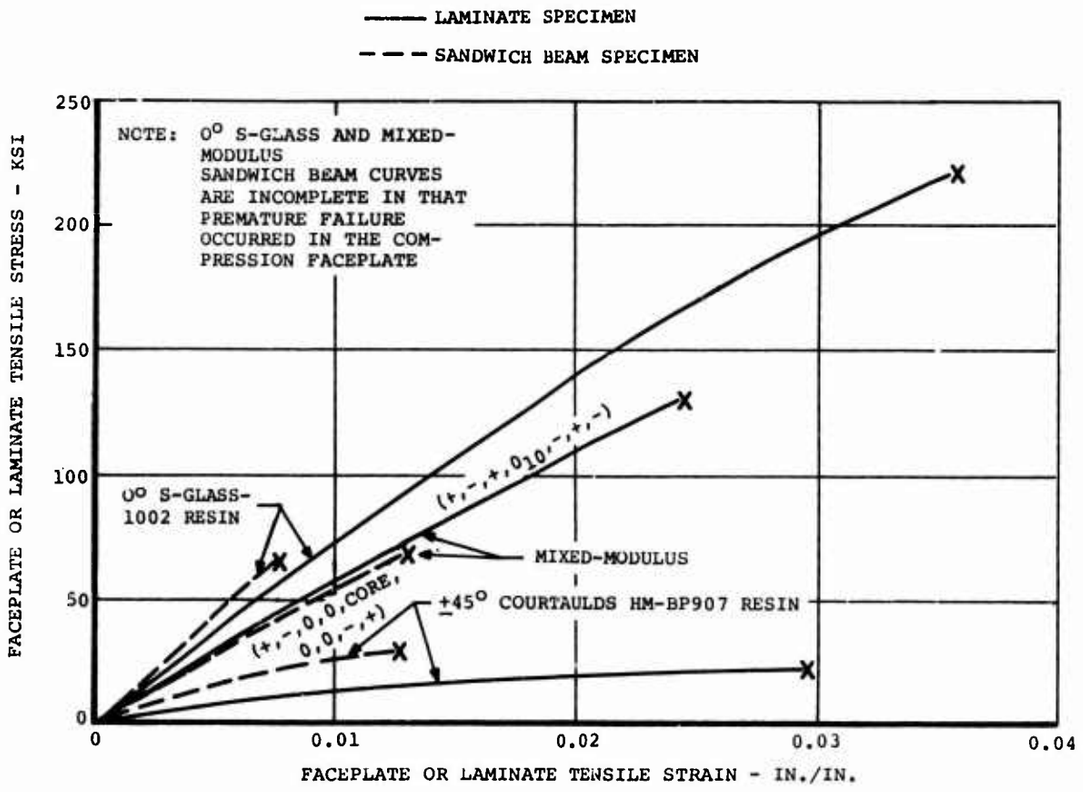

Figure 42. Comparison of Stress-Strain Curves for Laminate and Sandwich Beam Specimens.

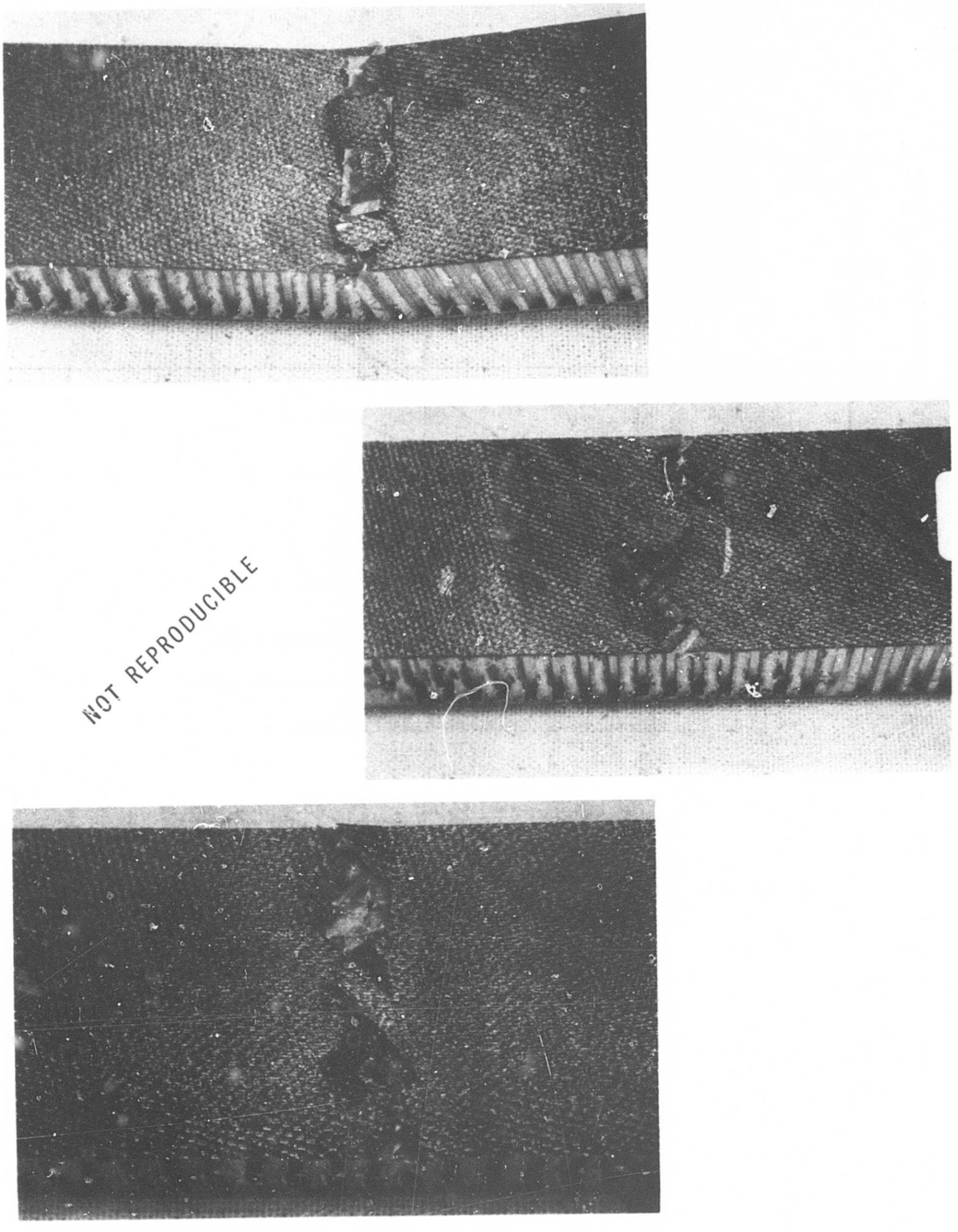

Figure 43. Typical Failed Static Mixed-Modulus Sandwich Beams.

the graphite layers to debond. Figure 44 shows typical ±45° graphite sandwich beam failures.

Dynamic Bending Tests

Flexural fatigue tests were conducted on the SF-1U fatigue machine (Figure 45). The test results for the mixed-modulus and the ±45° graphite beams are presented in Tables XV and XVI, with the S-N curves being shown in Figures 46 and 47. Note that the mixed-modulus sandwich beams (which had a 1-inch-thick, 12-lb/ft^3 5052 aluminum core with 1/8-inch cell and 0.003-inch wall thickness) were quite flexible and had a tendency to creep, eventually causing the test machine to "bottom out". In an effort to reach the desired stresses within the stroke limitations of the machine, the test length was shortened for specimens 101 through 113 in Table XV. Since these specimens did not have a stabilized core at the new grip location, most of them failed in the grip, which can be considered as a premature failure. However, in determining the "Mean of Test Data" curve in Figure 46, only those specimens which did not fail at the grip or bottom out were considered.

Because of a desire to prevent these same deflection problems for the ±45° graphite beams, the same honeycomb core was used with the exception that it was changed from 1 inch to 1-1/2 inches thick. This modification apparently worked. In determining the "Mean of Test Data" curve in Figure 47, no differentiation was assumed in the test data because of the different scrim constructions existing at the skin/core bond line.

Figure 48 compares the S-N results for the mixed-modulus, ±45° graphite and 0° S-glass sandwich beams. An S-N comparison of ±45° graphite sandwich beams with ±45° S-glass and ±45° boron sandwich beams is shown in Figure 49. Failure modes for the dynamically loaded mixed-modulus and graphite sandwich beams are similar to the photographs previously presented (Figures 43 and 44).

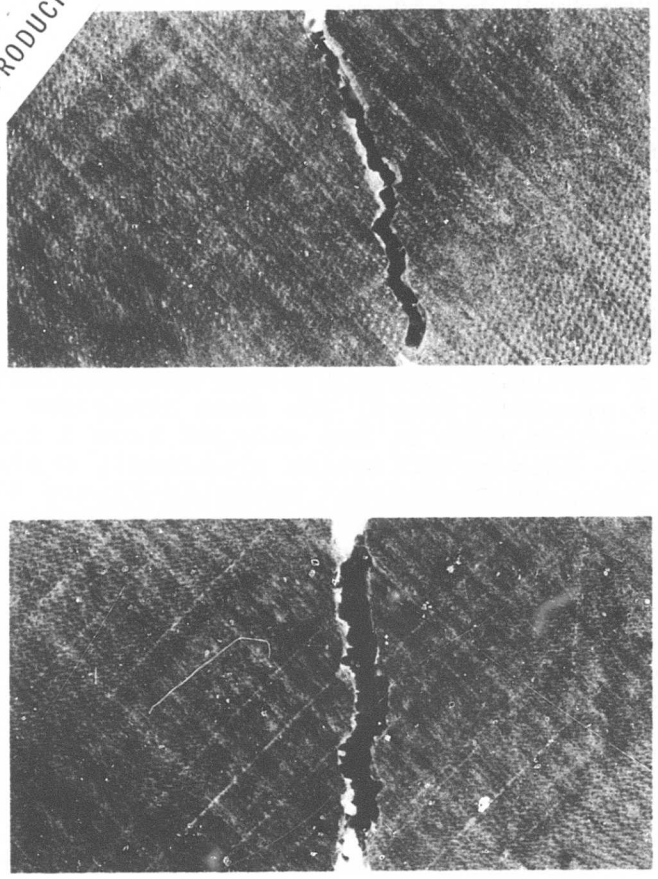

Figure 44. Typical Failed Static ±45° Graphite Sandwich Beams.

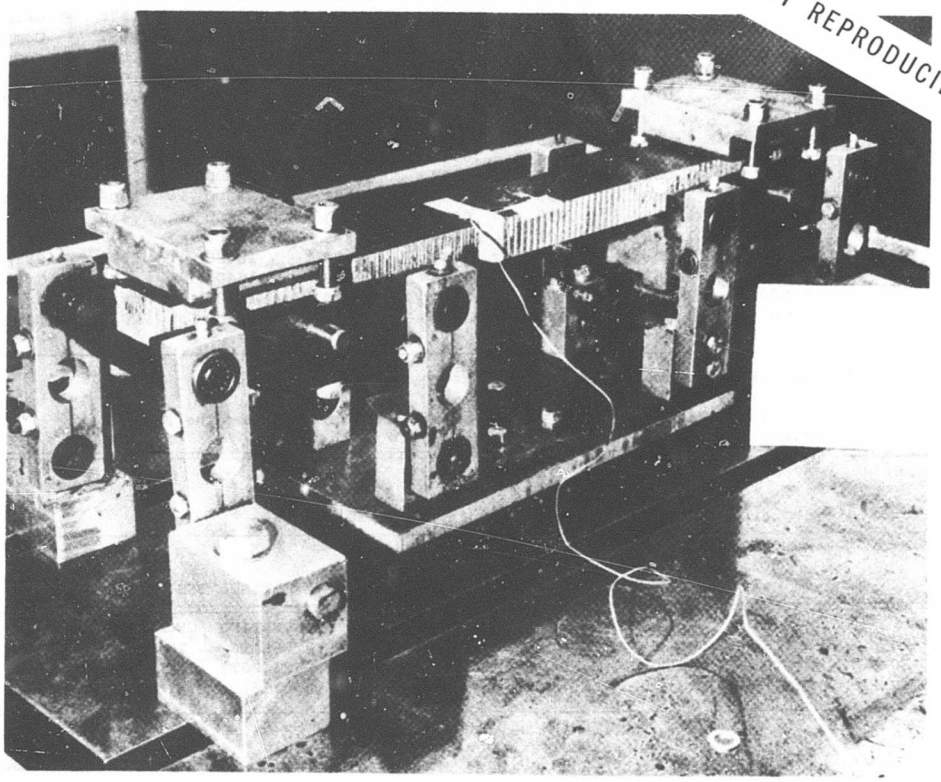

Figure 45. Typical Sandwich Beam Fatigue Test Setup.

TABLE XV. MIXED-MODULUS SANDWICH BENDING BEAM FATIGUE TEST RESULTS

SPECIMEN NUMBER	SPECIMEN WIDTH (IN.)	SANDWICH THICKNESS (IN.)	CORE THICKNESS (IN.)	FACE-PLATE THICKNESS (IN.)	MOMENT OF INERTIA ($IN.^4$)	ALTERNATING FACEPLATE STRESS (PSI) (R=0.05)	CYCLES TO FAILURE ($x10^{-6}$)	LOCATION OF FAILURE ORIGIN
2	1.797	1.070	1.003	.0334	.0323	24500	.003	Comp.Face
3	1.806	1.069	1.002	.0334	.0324	22500	.006	Comp.Face
4	1.794	1.070	1.003	.0334	.0323	20400	.234	Comp.Face
5	1.805	1.072	1.005	.0334	.0326	22100	.192	Comp.Face
8	1.797	1.071	1.004	.0334	.0324	21700	.174	Grip
9	1.796	1.070	1.003	.0334	.0323	22500	.092	Comp.Face
10	1.800	1.071	1.004	.0334	.0325	23300	.032*	Comp.Face
11	1.797	1.070	1.003	.0334	.0323	24500	.035*	Comp.Face
12	1.809	1.070	1.003	.0334	.0326	25300	.002	Grip
101	1.813	1.063	.996	.0334	.0322	22100	.014	Comp.Face
102	1.811	1.065	.998	.0334	.0323	22900	.048	Grip
103	1.804	1.066	.999	.0334	.0322	22500	.010	Comp.Face
105	1.806	1.066	.999	.0334	.0323	23300	.008	Grip
106	1.809	1.066	.999	.0334	.0323	18400	.439	Grip
107	1.812	1.068	1.001	.0334	.0325	18400	.247	Grip
109	1.806	1.068	1.001	.0334	.0324	18400	.394	Grip
110	1.805	1.067	1.000	.0334	.0323	16400	.726	Grip
111	1.809	1.067	1.000	.0334	.0324	16300	.951	Grip
113	1.806	1.064	.997	.0334	.0321	23300	.020	Comp.Face

*Invalid failures due to excessive deflection

Note: Only compression faceplate failures were used to generate the S-N curve of Figure 46.

TABLE XVI. ±45° GRAPHITE SANDWICH BENDING BEAM FATIGUE TEST RESULTS

	SPECIMEN NUMBER	SPECIMEN WIDTH (IN.)	SANDWICH THICKNESS (IN.)	CORE THICKNESS (IN.)	FACE-PLATE THICKNESS (IN.)	MOMENT OF INERTIA ($IN.^4$)	ALTERNATING FACEPLATE STRESS (PSI) (R=0.05)	CYCLES TO FAILURE ($x10^{-6}$)	LOCATION OF FAILURE ORIGIN
*	UF-1	1.993	1.564	1.503	.0306	.0715	8520	.025	Ten.&Comp. Faces
	-2	1.994	1.564	1.503	.0306	.0715	8010	.046	Core
	-3	1.996	1.563	1.502	.0306	.0715	7510	.012	Ten.&Comp. Faces
	-4	2.001	1.563	1.502	.0306	.0717	7020	.056	Ten.&Comp. Faces
	-5	1.995	1.563	1.502	.0306	.0715	6000	.350	Ten.&Comp. Faces
	-6	1.997	1.563	1.502	.0306	.0715	5010	5.073	Ten.&Comp. Faces
	-7	1.993	1.564	1.503	.0306	.0715	4010	10.207	Runout
	-8	1.994	1.562	1.501	.0306	.0713	4510	10.300	Runout
**	PF-1	1.990	1.571	1.506	.0326	.0766	4750	15.451	Runout
	-2	1.999	1.572	1.507	.0326	.0770	5700	10.300	Runout
	-3	1.995	1.573	1.508	.0326	.0769	6660	3.211	Ten.&Comp. Faces
	-4	2.001	1.571	1.506	.0326	.0770	7110	.143	Ten.&Comp. Faces
	-5	1.998	1.573	1.508	.0326	.0771	7600	.110	Ten.&Comp. Faces
	-6	1.999	1.572	1.507	.0326	.0770	8070	.041	Ten.&Comp. Faces
	-7	1.995	1.572	1.507	.0326	.0768	6400	.762	Ten.&Comp. Faces
	-8	1.980	1.569	1.504	.0326	.0760	6160	.301	Ten.&Comp. Faces

Adhesive between faceplates and core:

* - ±45° Graphite Faceplate
- 1 Ply BP907 Unsupported Resin
- 1 Ply Dry 104 Glass
- Aluminum Honeycomb Core

** - ±45° Graphite Faceplate
- 1 Ply BP907-120 Prepreg
- 1 Ply AF126 Adhesive
- Aluminum Honeycomb Core

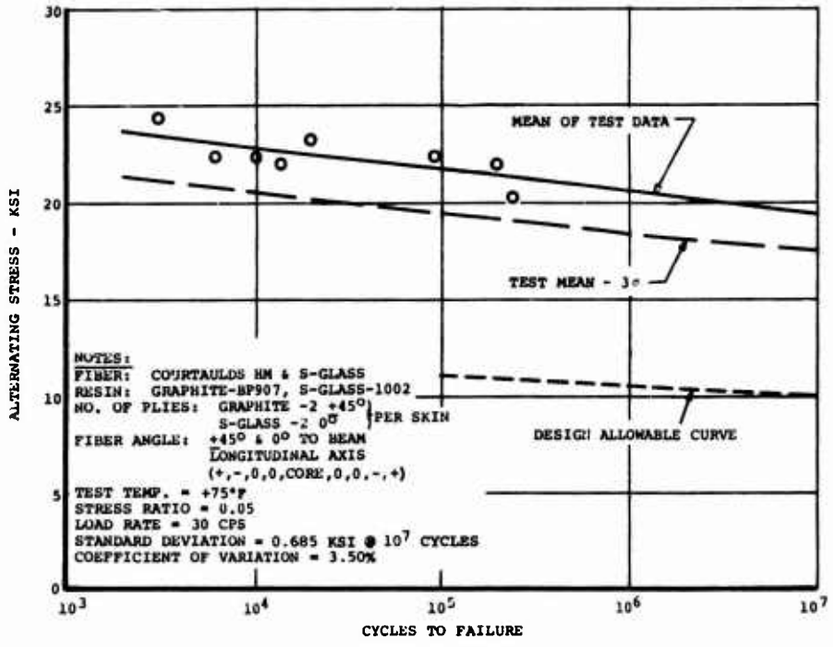

Figure 46. S-N Curve for Mixed-Modulus Sandwich Bending Beams.

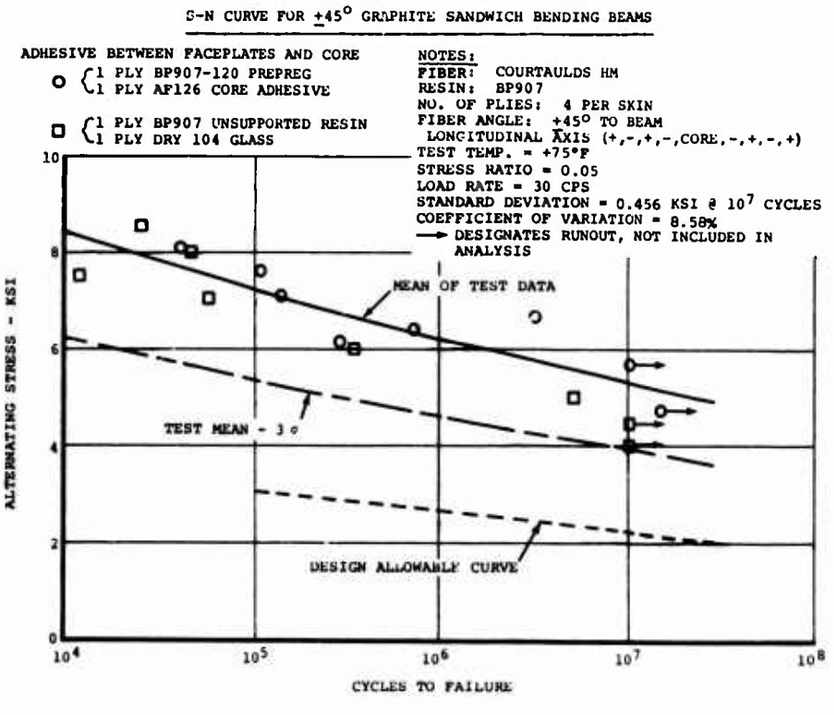

Figure 47. S-N Curve for ±45° Graphite Sandwich Bending Beams.

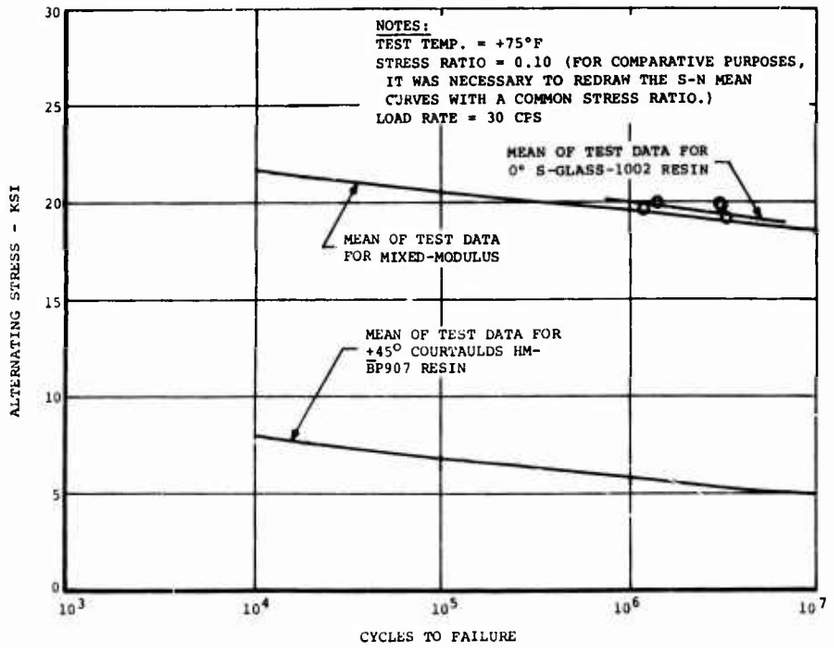

Figure 48. S-N Comparison of Mixed-Modulus, ±45° Graphite, and 0° S-Glass Sandwich Bending Beams.

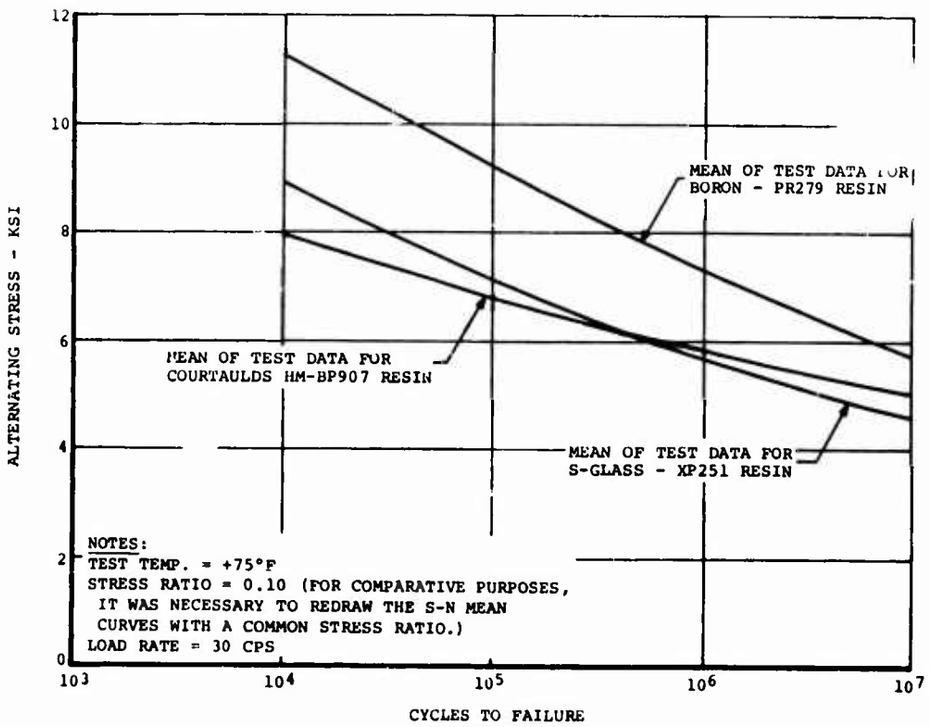

Figure 49. S-N Comparison of ±45° Graphite, S-Glass, and Boron Sandwich Bending Beams.

CONCLUSIONS

Evaluation of the test data reveals that initial static failure of any of the three specimen configurations considered (tensile laminates, tubes, or sandwich beams) occurs in the graphite-epoxy element due to a strain mismatch between angle-ply graphite and uni S-glass. In the laminates, the full strain capability of the glass was not realized before the graphite angle-ply failed; thus, the graphite strain field is the critical design criterion. For the torsion tube, the graphite angle-ply strain was again the critical design criterion, even though the ultimate shear stress was obtained at a greater strain than that of an all-angle-ply graphite tube due to geometric effects. The fatigue stress level in the mixed-modulus faceplate of the sandwich beams appeared to be higher than that anticipated when compared to the unidirectional, 0° S-glass sandwich beams. Further analysis of the sandwich beam data might provide an explanation of this behavior.

All failures are believed to be valid ones in that there does not appear to be any strong evidence of resin incompatibility or any detectable evidence of curing damage due to the large differences between the coefficients of thermal expansion of the two materials (see the Appendix). For tensile loadings, however, restrictions must be placed on the ratio of the glass-epoxy cross-sectional area to that of the graphite-epoxy so that catastrophic failures do not occur once the graphite angle-ply fails.

Results to date indicate that the compatibility of mixed graphite-glass composites will be feasible for use in an all composite full depth honeycomb rotor blade. It is therefore recommended that mixed-modulus development be continued with emphasis on optimizing the system for specific design applications. It is recognized, for instance, that the resin systems used were not intended for high temperature applications (i.e. > 160°F). There are other known resin systems which have similar strain capability to the 1002 and BP907 resins and which can be formulated for higher temperature applications.

To increase design utility, it is recognized that other than full depth honeycomb monolithic structures will be required. The use of built-up structures (i.e. sandwich skin, rib spars, etc.) will require development of suitable attachment techniques. Presently, no data exists for adhesively bonded or mechanically fastened joints utilizing a mixed-modulus composite system.

An important design application is the use of thin sandwich structures (i.e. fuselage panels or blade boxes, which were not envisioned in this program. These structures would be more

susceptible to warpage induced by the difference in coefficient of thermal expansion between the two composite constituents of the mixed-modulus system. Solutions for alleviating this potential problem should be investigated.

APPENDIX

POST-FAILURE MICROSCOPIC EXAMINATION

Two static specimens consisting of a torsion tube and a deflection laminate, which was subsequently failed in static tension,* were selected for examination using the Scanning Electron Microscope (SEM).

Two types of fractures were available with these specimens: those occurring (a) at the interface between the $\pm 45°$ graphite and the uni S-glass and (b) transverse to the local fiber orientation. The fractographic documentation of these failure regions is shown in Figures 50 and 51 for the deflection and tube specimens, respectively. Figure 52 presents a photomicrograph of the deflection laminate showing typical fiber distribution.

At low optical magnifications, the interface fractures appeared to have isolated patches of the opposing composite's resin and fibers left clinging to the surface. The SEM investigation not only verified this observation (Figures 50a, 50b, and 51b) but also revealed a large number of denuded S-glass and graphite fibers (Figures 50 and 51). A fracture parallel to the interface would naturally result in a large number of exposed fibers. The extent to which the fibers are denuded here indicates that the fiber-resin interface bond was the weak link in both the graphite and glass systems.

The results indicate that the cohesive strength of the composite exceeded the adhesive strength for both resin systems. This is observed on the normal fracture surface of Figures 50c, 50d, and 51e, in which the crack is shown to predominantly follow the resin-fiber interface. If the reverse were true, i.e. the adhesive strength were greater than the cohesive strength, the failure surfaces would tend to be more planar. These same micrographs also confirm good resin penetration of the fiber strands; hence, the excessive number of denuded fibers cannot be attributed to this source. One further point concerning resin incompatibility can be raised. Figures 50a and 50b contain no evidence of resin mismatch, since the failure plane is shown not to reside at the BP907 - 1002 resin interface. Rather, the fracture has propagated along the resin-fiber interface of one or the other of the two composites. From this observation, it may be assumed that the resin interface strength was greater than the adhesive strength of either of the composite systems.

*This specimen's fracture appeared similar to the fractures of the pure static specimens depicted in Figure 6.

Evidence of a weak resin-fiber interface bond is not necessarily indicative of a poorly manufactured specimen with a built-in failure mode. What is shown here is that, of the three mechanisms of composite degradation (fiber breaks, resin-fiber interface fracture, and resin fracture), the resin-fiber interface failure dominated in the mixed-modulus specimens examined.

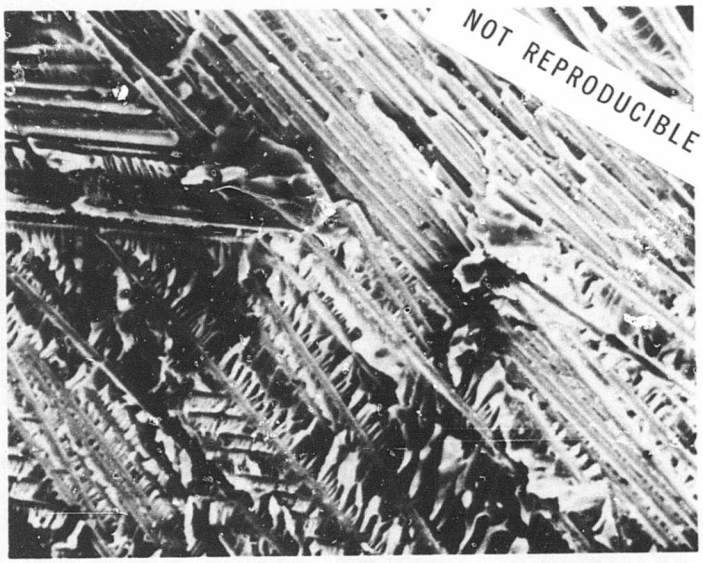

(a) 190X GRAPHITE (——) S-GLASS (\)

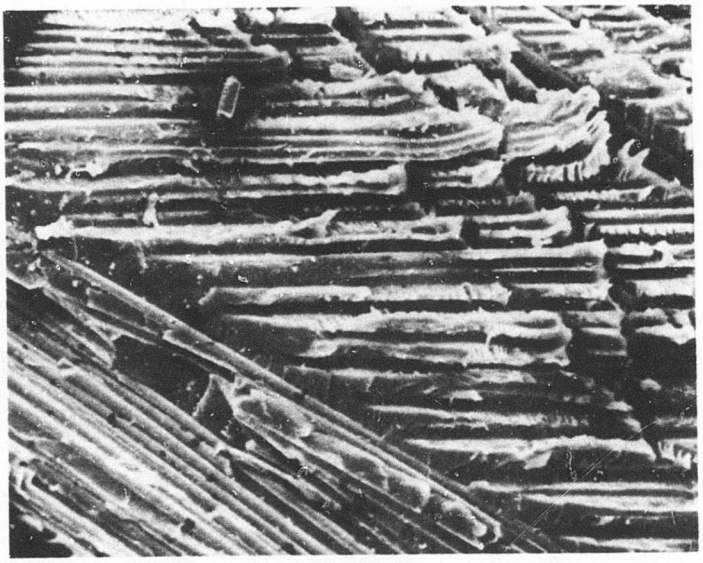

(b) 200X GRAPHITE (——) S-GLASS (\)

Figure 50. Scanning Electron Micrographs of a Failure Surface from a Static Mixed-Modulus Deflection Specimen.

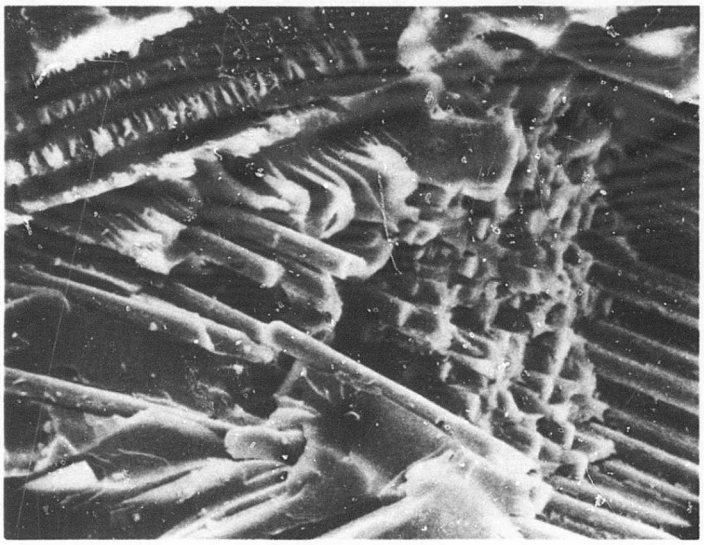

(c) 380X S-GLASS

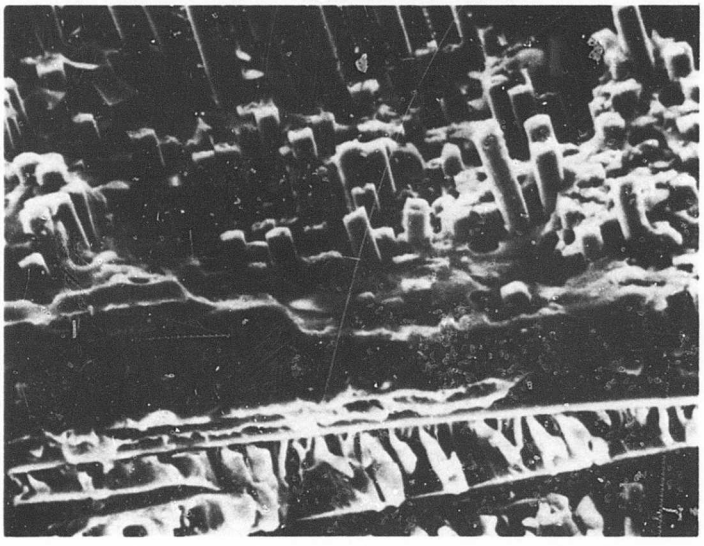

(d) 390X GRAPHITE (——) S-GLASS (\ )

Figure 50. (cont.)

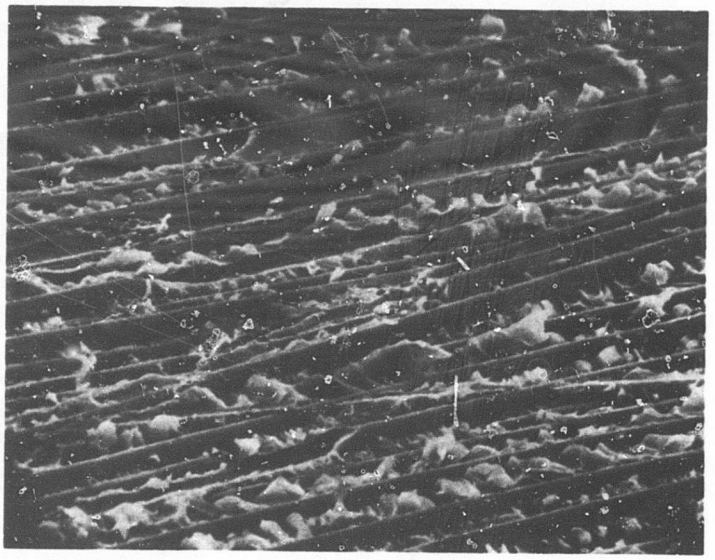

(e) 410X S-GLASS

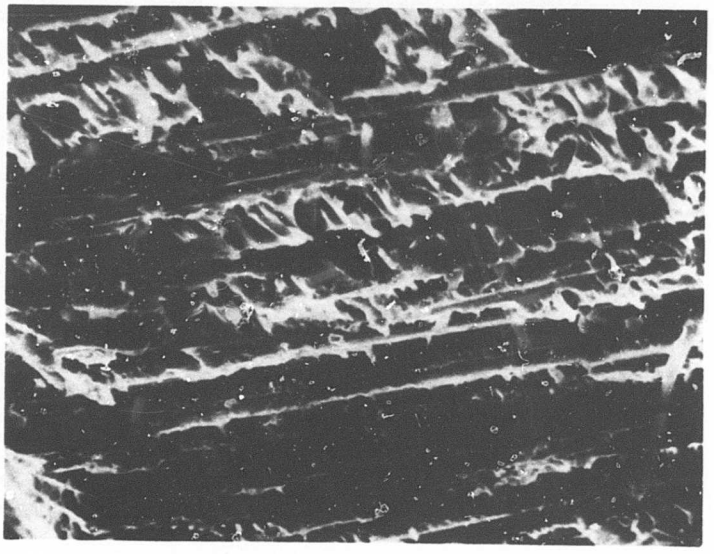

(f) 410X GRAPHITE

Figure 50. (cont.)

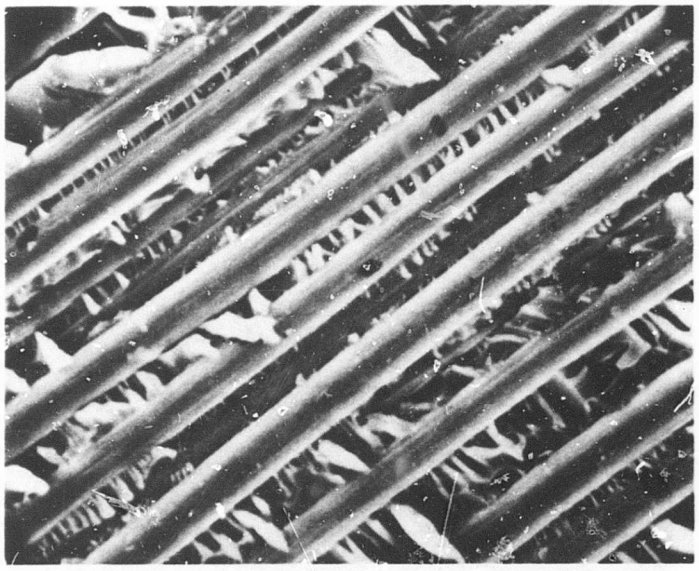

(g) 760X S-GLASS

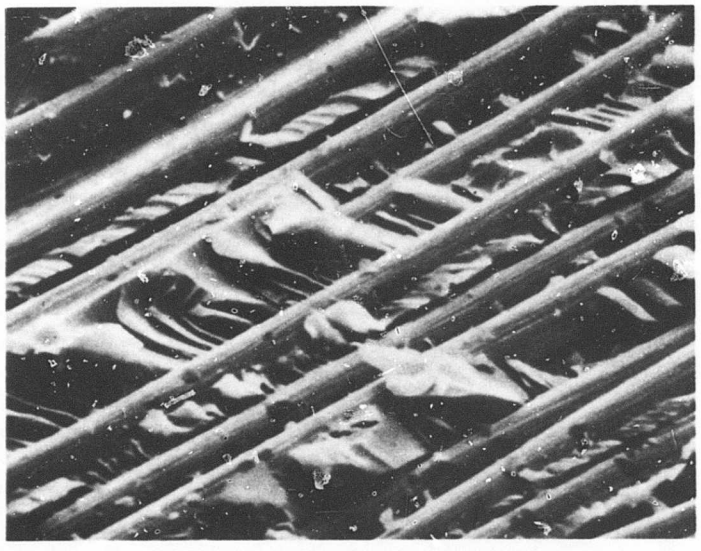

(h) 800X S-GLASS

Figure 50. (cont.)

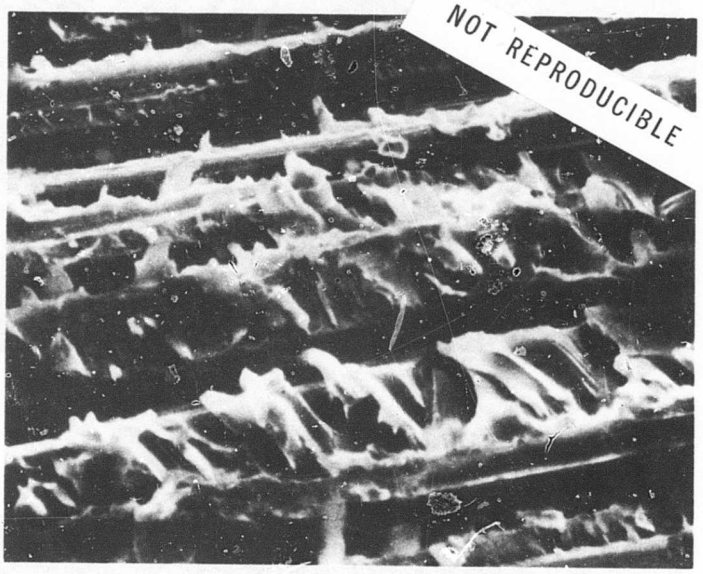

(i) 820X GRAPHITE

Figure 50. (cont.)

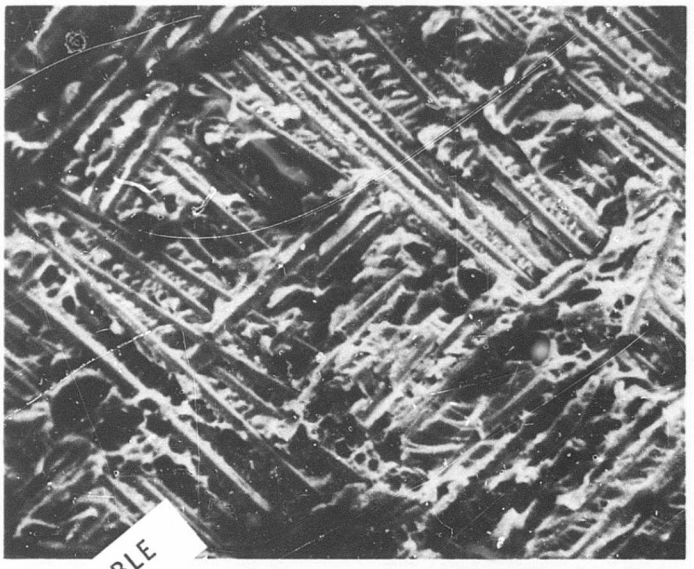

(a) 220X GRAPHITE

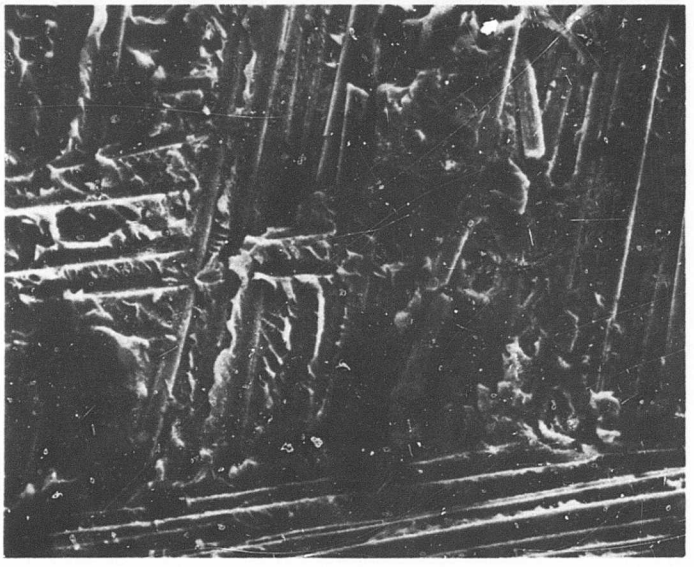

(b) 330X GRAPHITE (—) S-GLASS (/)

Figure 51. Scanning Electron Micrographs of a Failure Surface from a Static Mixed-Modulus Torsion Tube Specimen.

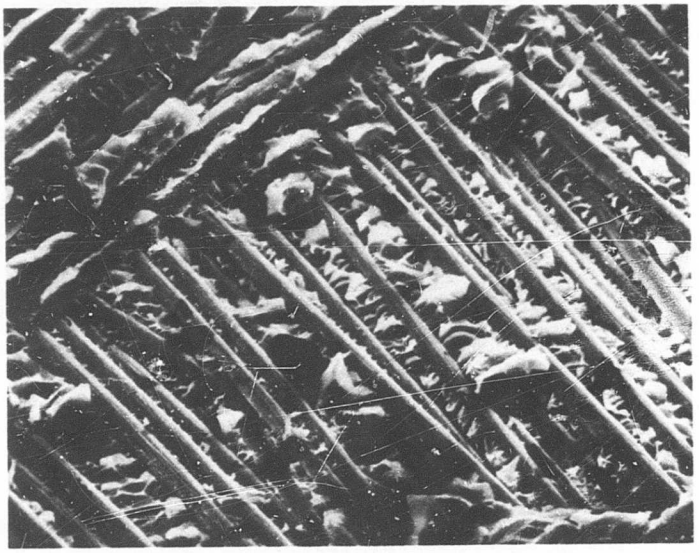

(c) 400X GRAPHITE

Figure 51. (cont.)

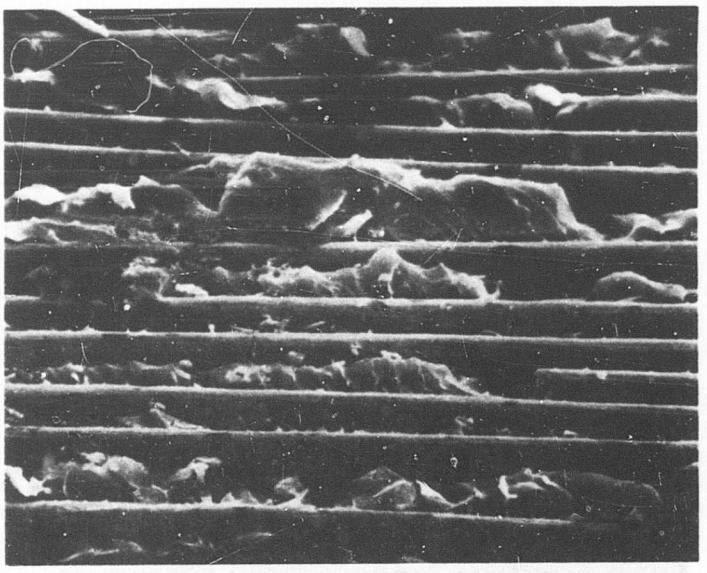

(d) 700X GRAPHITE

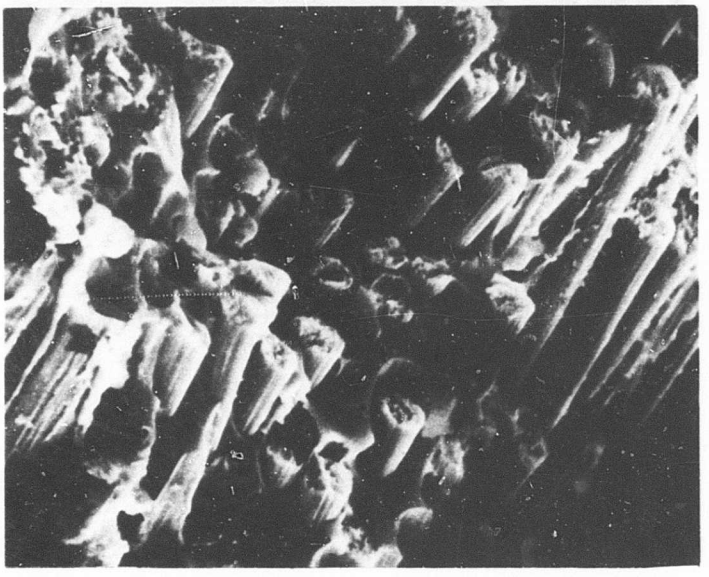

(e) 800X GRAPHITE

Figure 51. (cont.)

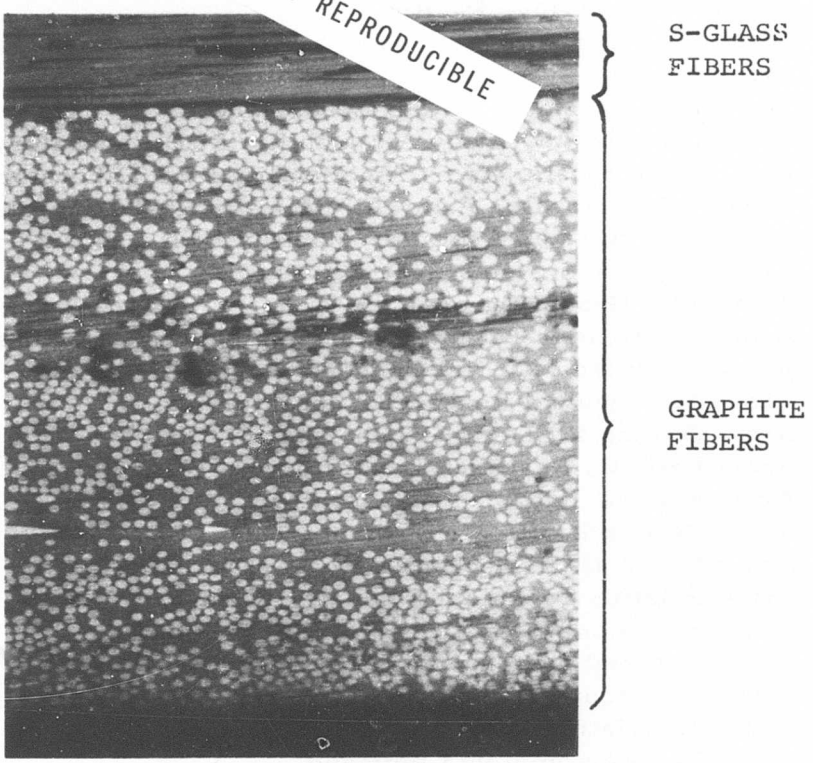

Figure 52. Photomicrograph of a Static Mixed-Modulus Deflection Specimen Showing Typical Fiber Distribution.